Detailed Observations made at High Incidences and at High-Subsonic Mach Numbers on Goldstein 1442/1547 Aerofoil

By

H. H. PEARCEY, B.Sc., and Miss M. E. FABER,
of the Aerodynamics Division, N.P.L.

Reports and Memoranda No. 2849*
November, 1950

Summary.—Detailed measurements, including surface-pressure distributions, shock-wave photographs and observations of boundary-layer separation, have been made over a wide range of incidence in the National Physical Laboratory 20-in. × 8-in. High-Speed Wind Tunnel on the Goldstein 1442/1547 aerofoil NPL 177, previously tested at lower incidences in this tunnel.

The tests have shown that with standard models of 5-in. chord the stall can be covered for Mach numbers up to nearly 0·8 unless it is delayed beyond the usual incidence range, as for Mach numbers above 0·7 for the present section. For these cases, however, it should still be possible to cover the useful range of C_L which is often limited by other considerations, *e.g.*, pitching-moment coefficients.

The observations enable the effects of compressibility on $C_{L\ max}$ and on the nature of the stall to be studied in detail for the two-dimensional case. The pitching-moment coefficients, also, can be integrated from the pressure distributions. Since the main purpose of experiments of this type is to provide qualitative explanations of the compressibility effects, the limitations on the accuracy of the results due to tunnel interference and the fairly low Reynolds numbers (1·0 to 1·8 × 10^6) are not likely to detract seriously from their value.

Certain features of the results on the Goldstein section are thought to be of fairly general interest and application. These include :

(*a*) The occurence, for free-stream Mach numbers of 0·55 and above, of a very rapid supersonic expansion, probably around the bubble formed by a local separation or thickening of the boundary layer near the nose. This is accompanied by an increase in the maximum local Mach number and a fairly abrupt rise in $C_{L\ max}$. It tends to confirm an explanation which has been suggested for the beneficial effect of a small leading-edge radius on $C_{L\ max}$ at high speeds.

(*b*) The increasing tendency to stall due to the boundary-layer thickening at the foot of the shock-wave. The increase in the extent of this thickening with increasing incidence is sufficient, for Mach numbers above 0·5, to cause the aerofoil to stall at a reduced incidence where the magnitude of the pressure recovery on the upper surface is hardly changing.

(*c*) The changes in flow pattern which lead to the absence of a maximum in the lift *vs.* incidence curves for Mach numbers of about 0·75 and above, a feature noted in many other tests. The present measurements show, however, that the useful lift would probably be limited by a rapid increase in nose-down pitching moment.

* Published with the permission of the Director, National Physical Laboratory.

CONTENTS

1. *Introduction.*—Beavan and Hills[1] have drawn attention to the possibility of studying the effects of compressibility at high incidences by pressure plotting and other observations of flow on 5-in. chord aerofoils in the National Physical Laboratory 20-in. × 8-in. High-Speed Wind Tunnel. They felt that such tests should help to elucidate the underlying causes of the variations in $C_{L\max}$ for the fundamental two-dimensional case at high subsonic Mach numbers and should yield other useful results, including the variation of pitching moment near the stall. They suggested that, in order to illustrate the beneficial effects on $C_{L\max}$ at high speeds of reduced nose radius, of camber, of reduced thickness and of far back maximum thickness, the tests on a systematic series of aerofoils[2] should be extended to high incidences. Considerable delay was anticipated in the construction of the models of this series and so, in order to explore the possibilities of the technique, an opportunity of a short gap between other items on the tunnel programme was used to make some preliminary observations on the Goldstein 'Roof-Top' section, 1442/1547 (N.P.L.177), previously tested at lower incidences[3]. In particular it was hoped to find how far the range of Mach number and incidence would be restricted by tunnel choking and by limitations in model strength, and whether the stall could be covered adequately.

The limitations imposed by the tunnel constraint, spanwise variations of flow, low Reynolds numbers, etc., on the accuracy of the observations are discussed in the present report.

Although the Goldstein section is of a type and thickness not consistent with recent trends in high-speed section design, the results are presented because they show that the variation of $C_{L\max}$ with Mach number, which is similar to that for many other sections, can be explained qualitatively from the detailed observations. The variation of pitching-moment coefficient at high incidences is also shown, which is of itself quite important and of which there are few results available. Further, the detailed observations reveal certain flow phenomena which are thought to be significant and may be of more general application and interest.

As far as is known, few pressure distributions accompanied by photographs of shock-waves, etc., for high incidences and Mach numbers have been published, and so these observations are given and described fairly fully for the present case. It is hoped that they may help in the understanding of the varying nature of the stall and of other effects of increasing Mach number in this régime, and in the planning of further work on these problems. The pressure distributions also afford details of loading which should be useful for stress purposes.

The main aspects of the results are summarized and their significance remarked upon in section 7.

2. *Experimental Details.*—2.1. *Tunnel, Model, etc.*—The tunnel, pressure-plotting technique and method of model construction have been described fully by Holder[4] and it will be sufficient here to mention certain relevant details.

The Reynolds number varied from $0{\cdot}8 \times 10^6$ at the lowest Mach number, $0{\cdot}3$ to $1{\cdot}8 \times 10^6$ at $M = 0{\cdot}8$ (*see* Fig. 2).

The tunnel span and aerofoil chord were 8 in. and 5 in. respectively; the tunnel height was 17·5 in.

Owing to the difficulties of setting the flexible walls to 'streamline' shapes for extreme incidences within the restricted length of working-section available, these 'streamline' settings[5] were not used. The walls were set instead to give constant velocity along the tunnel in the absence of the model, *i.e.*, straight walls with taper to allow for boundary-layer growth. Datum static pressure was measured at a point on one flexible wall, about two chords upstream of the leading edge of the model.

Details of the Goldstein Roof-Top section, 1442/1547, are given in Ref. 3 ; a drawing of the profile showing the chordwise location of the pressure holes is reproduced in Fig. 1. These pressure holes were distributed over the middle $3\frac{1}{2}$ in. of the 8-in. span.

2.2. *Observations.*—Surface pressures were measured enabling normal-force and pitching-moment coefficients to be evaluated and detailed pressure distributions to be studied. These were supplemented in many cases by direct-shadow photographs which show the shock-waves clearly and some details of the boundary-layer flow. It was possible to obtain, subsequent to the main tests, more precise information on boundary-layer separation for a few representative cases from observations of oil on the surface and from Toepler schlieren photographs. Turbulent separations were accompanied by reversed flow from the trailing edge and the oil gave a fairly reliable indication of these. Local laminar separations followed by re-attachment were more difficult to determine precisely, especially when the separation was effectively a small bubble very near the leading edge ; there may have been cases where these were present but not observed when the oil was used.

The range of incidence obtainable was sufficient to cover the stall for Mach numbers up to 0·7. For higher Mach numbers there was a change in the type of C_N vs. α curve and there was no stall below the maximum C_N permissible from strength considerations. A limit of 200 lb on the normal force was imposed in order to ensure a safe stress in the supporting pins ; the corresponding limiting C_N varied from 1·25 at $M = 0{\cdot}75$ to 1·16 at $M = 0{\cdot}8$.

3. *Presentation of Results.*—The normal-force coefficients, C_N, and quarter-chord pitching-moment coefficients, C_m, are all given in Fig. 3 plotted against incidence for constant Mach numbers. The normal-force coefficient C_N, is very nearly the same as the lift coefficient C_L. for small incidences ; the differences at the highest incidences of these tests do not exceed 2 per cent. For greater accuracy in the curve of $C_{L\,\max}$ against M, Fig. 4a, the longitudinal forces were integrated near the stall enabling the differences between C_N and C_L to be found in this region. The angle for maximum C_L is given in Fig. 4b.

The variation of $C_{L\,\max}$ for the present section is compared in Fig. 5a with the results of tests on similar sections.

The pressure distributions, in the form of pressure coefficients C_p, are plotted for several incidences at each of several Mach numbers in Figs. 11 to 22a. Direct-shadow photographs are given in Figs. 12b, 14b and 14c, 16b to 20b and 22b. Schlieren photographs for two incidences at $M = 0{\cdot}5$ are given in Fig. 14d, for one incidence at $M = 0{\cdot}65$ in Fig. 17c, and for various Mach numbers at $\alpha = 6{\cdot}5$ deg in Fig. 25. A control, direct-shadow, photograph without airflow is given in fig. 30 to show the positions of supports, etc., and imperfections on the glass. The pressure distributions for varying Mach number are collected in Figs. 6 to 9, Fig. 6 showing, for each Mach number, the distribution for the nearest angle to the stalling angle at which observations were made, and Figs. 7, 8 and 9 the distributions for the incidences of 8·5 deg, 10·5 deg and 12·5 deg. The minimum pressure coefficient on the upper surface is plotted against free-stream Mach number in Fig. 10 for incidences near and at the stall. The local Mach numbers M_L, plotted on this figure and indicated on most of the pressure distributions are related to the pressure coefficient on a theoretical basis assuming isentropic flow and are therefore strictly accurate only upstream of shock-waves.

The approximate positions of boundary-layer separations determined by the observations with oil are given in Table 4.

Certain of the pressure measurements and other detailed observations are presented in different forms in Figs. 23 to 29 which will be referred to in the discussions.

4. *Accuracy of Results.*—4.1. *Effect of Tunnel Interference.*—The ' streamline ' settings of the flexible walls were not used (*see* section 2.1 above) and the results are therefore subject to the effect of tunnel constraint for a straight-walled tunnel.

It has not been possible to apply the appropriate two-dimensional corrections to all of the observations as drag measurements, necessary for the evaluation of wake blockage, were not obtained. Calculations have been made, however, for two incidences, 0·5 deg and 6·5 deg, using drags estimated from the results of earlier tests. Specimen corrections on Mach number, pitching-moment coefficient and incidence and the ratios of corrected to uncorrected normal-force coefficients are given in Table 1, the corrected values being indicated by primed symbols.

TABLE 1

M	$\alpha = 0{\cdot}5$ deg				$\alpha = 6{\cdot}5$ deg			
	$M' - M$	C_N'/C_N	$\alpha' - \alpha$ (deg)	$C_m' - C_m$	$M' - M$	C_N'/C_N	$\alpha' - \alpha$ (deg)	$C_m' - C_m$
0·3	0·001	0·98	0·01	0·001	−0·003	1·01	0·11	0·003
0·5	0·003	0·97	0·01	0·002	−0·001	0·99	0·14	0·004
0·7	0·009	0·95	0·01	0·003	0·004	0·96	0·21	0·007
0·75	0·014	0·94		0·003	0·015	0·94	0·15	0·009

The corrections on Mach number allow for the ' blockage ' of the model and its wake and also for an error in datum pressure due to a slight gradient across the tunnel which increased with incidence. The effects of these on the dynamic pressure have been incorporated in the corrections on the force coefficients which allow also for the effective change in camber due to the curvature of the flow. The effective change in incidence due to this curvature is compensated for in the incidence correction. The formulae used and the appropriate references are listed in Appendix I.

The values in Table 1 suggest that the correction on Mach number does not change greatly with incidence and therefore that the Mach number is sensibly constant for those figures in which the observations are plotted for fixed values of the uncorrected Mach number. The main effect of the corrections on normal-force coefficient and incidence would be to reduce slightly the variation of the coefficient with incidence at constant Mach number, or with Mach number at constant incidence. It is considered, however, that none of these corrections would have any appreciable influence on the qualitative discussion of the results particularly as regards the development of flow characteristics with changing Mach number or incidence. This applies also to the corrections which should strictly be made to the coefficients derived from the surface pressures but which have been omitted in presenting the pressure distributions.

For the maximum lift coefficients, on the other hand, there is likely to be more interest in comparison of the actual values with results obtained elsewhere, so that it is desirable to correct them for tunnel interference if possible. The same formulae have been used but their validity probably becomes more doubtful at the high incidences[22]. The corrected values of Mach number, $C_{L\,\max}$ and incidence for maximum lift coefficient have been used in Figs. 4 and 5, and the magnitude of the corrections is indicated in Table 2. (For the calculation of the wake blockage, the form drag was used, on the basis that the difference between this and the profile drag should be relatively small at high incidences.)

TABLE 2

M	$M' - M$	$C_{L\,\max}'/C_{L\,\max}$	$\alpha' - \alpha$ (deg)
0·3	0·001	0·98	0·17
0·5	0·003	0·97	0·22
0·6	0·005	0·96	0·24
0·7	0·015	0·93	0·20

The magnitudes of all the above corrections increase with Mach number and become invalid as the choking Mach number is approached. For the main body of results an arbitrary limit on Mach number and incidence has been imposed and no cases included for which the local supersonic region above the aerofoil stretched to the tunnel wall. Observations under these conditions may, however, be of qualitative interest in illustrating probable flow trends at higher Mach numbers than could otherwise be obtained, and have been included in Fig. 3, the curves being shown dashed in this region, and also in Figs. 20, 22, 26, 27 and 29.

The errors of C_L due to the loss of lift at the ends of the aerofoil in the side-wall boundary layers have been shown in recent investigations, *e.g.*, Ref. 23, to be negligible at moderate incidences, even for the fairly low span/chord ratio used here. They may become more serious at very high incidences, however, especially if there is a tendency towards a premature stall at the ends. For the present tests there appears, in fact, to be a narrow range of Mach number around 0·7 for which flow conditions near the leading edge are critical at high incidences. With increasing Mach number in this region there is a tendency for the flow to change from stalled flow near the nose to flow with the boundary layer adhering and supersonic velocities persisting back to about mid-chord. This is shown, for example, in the photographs for $\alpha = 10{\cdot}5$ deg, $M = 0{\cdot}65$, 0·7, 0·75 and 0·775 in Figs. 17b, 18b, 20 and 22 respectively, the shock-wave and rapid boundary-layer thickening occurring very near the leading edge at $M = 0{\cdot}65$ and progressively further back as the Mach number is increased. The flow conditions are most critical at 0·7 where this trend first starts, and spanwise variations in the positions of the shock-waves and of the boundary-layer stalling are evident in the photographs in Fig. 18b for this Mach number and incidences above 9·5 deg. These are thought to occur because of the adhered flow being more easily established over the centre of the span than near the ends.

Conditions were probably constant over the centre $3\frac{1}{2}$ in. in which the pressure holes are positioned so that readings of these would not have been directly affected by the stalled flow at the ends, but the existence of the spanwise variations in loading may well have led to serious induced effects and errors on measured C_L.

The flow pattern with these spanwise variations probably resembles the spanwise variations explored in detail by Todd[24] during high-speed tests on a cascade of highly cambered aerofoils. The errors in those tests would, of course, have been much larger than for the present case because the curvature of the flow was greater and the span/chord ratio less.

The main effect of these variations is probably to reduce slightly the Mach number at which the adhered flow becomes established and hence that at which the lift curve without a peak first occurs (see later). Their influence is likely to be restricted, however, to the narrow range of Mach number in which the flow changes near the nose first appear. Below and above these Mach numbers the spanwise variations are less noticeable ; in the present case, for example, the adhered flow is fairly well established over the front half of the aerofoil for $M = 0{\cdot}75$ and 0·775 and the spanwise variations greatly reduced.

4.2. *Effect of Reynolds Number.*—The effect of Reynolds number may be important in two ways which have been discussed[6 to 12] fairly fully in relation to other experiments under similar conditions.

Firstly, since the stagnation pressure is constant, the Reynolds number varies simultaneously with the test Mach number, Fig. 2, and although the variation of the former is fairly small, the effects of the two variables may be confused. The effect of increasing Reynolds number at constant Mach number, for an aerofoil of moderate thickness and within the range of the present tests, is likely to be an increase in $C_{L\,\max}$, due to the decrease in the extent of the bubble formed by the local separation of the laminar boundary layer near the nose and the resulting more favourable initial conditions of the re-attached turbulent layer[6,13]. Increasing Mach number in the low range, *i.e.*, up to about 0·5 for the present section, at constant Reynolds

number produces, on the other hand, a decrease in $C_{L\,max}$[9]. Thus, for a test in which the two variables increase simultaneously, conflicting effects are to be expected. It has been found[10,11,12] that at first Reynolds number is the more important and that there is a rising $C_{L\,max}$ up to a certain Mach number. Above this the compressibility effects become more important and $C_{L\,max}$ begins to decrease. For still higher Mach numbers the effects of the variation in Reynolds number seem to become negligible in comparison with those due to Mach number. For the present tests it is considered that the effect of the varying Reynolds number predominates up to $M = 0{\cdot}4$ but is unimportant above this value (*see* section 4.1).

Secondly, the values of Reynolds number are low compared with full-scale and, although the results may give a good indication of the effects of compressibility at low Reynolds numbers, it is well to bear in mind that these effects, and also the overall values of $C_{L\,max}$ and force coefficients, may be different at higher values. The available evidence[7,8,9] suggests that the variation with Mach number remains qualitatively the same at the increased Reynolds numbers and further that there may be practically no effect of Reynolds number on the overall values of $C_{L\,max}$ at Mach numbers above about $0{\cdot}55$. This decreasing influence of Reynolds number is probably due to the fact that the position and manner of boundary-layer separation is largely determined in relation to the shock-wave positions rather than the more normal factors important at low speeds. The evidence is not complete, however, and in view of recent findings that the shock-wave positions and patterns can be considerably affected by the boundary layer, there is the possibility that a Reynolds number effect of a different kind may exist under certain conditions. There was, in fact, a suggestion of this for one of the tests considered in Ref. 9.

5. *Force Coefficients.*—5.1. *Normal-Force.*—The curves of normal-force coefficient C_N, plotted against incidence for constant free-stream Mach numbers, Fig. 3, show definite peaks for all Mach numbers up to $0{\cdot}65$. These peaks are not particularly sharp and suggest a fairly gradual stall.

The peak is absent at $M = 0{\cdot}7$, and, after falling roughly to zero at about 10 deg, $\partial C_N/\partial\alpha$ increases again instead of becoming negative. The value of C_L at the incidence at which $\partial C_N/\partial\alpha$ is nearly zero has been taken as the $C_{L\,max}$ for this Mach number.

For higher Mach numbers there is no sign of a maximum in the C_N vs. α curves within the range of incidence covered, *i.e.*, up to $13{\cdot}5$ deg for $M = 0{\cdot}75$, 12 deg for $M = 0{\cdot}775$ and $7{\cdot}5$ deg for $M = 0{\cdot}8$, including those cases for which the local speed of sound reaches the tunnel wall. This behaviour is similar to that observed[7,8] for several other sections at these Mach numbers, but for much smaller models in the same tunnel, and is not thought to be caused by the constriction of the flow. The Mach number for which the peak is first absent may, however, be affected, particularly by the end effects (*see* section 4.1).

The changes in lift-curve slope at low Mach numbers, starting at about 4 deg to 6 deg incidence, are similar to those observed elsewhere for similar low-drag sections[10,14]. Observations of the flow (*see* later) confirm the suggestion in Ref. 10 that they are due to the building up of boundary-layer separation over the rear part of the upper surface. The separation disappears in the small range of Mach number between $0{\cdot}6$ and $0{\cdot}7$, following the rearward movement of the shock-wave, and the changes in $\partial C_N/\partial\alpha$ become less noticeable. Further comments on the variations in lift-curve slope and on the observations of boundary-layer separation are given in Appendix III.

5.2. *Pitching Moment.*—The curves of quarter-chord pitching-moment coefficient, C_m, show that for Mach numbers up to $0{\cdot}65$ there is a negative, *i.e.*, nose-down, moment at low incidences, the magnitude of which decreases gradually with increasing incidence up to the stall; a rapid increase of nose-down moment begins at the stall. For Mach numbers of $0{\cdot}7$ and above the rate of increase of nose-down moment becomes very large at high incidences even in the absence of a peak in the C_N vs. α curve.

5.3. $C_{L\max}$.—The value of $C_{L\max}$ remains fairly high, Fig. 4a, in the range of Mach number where there is an obvious stall, there being no drastic falling off, except perhaps between $M = 0{\cdot}65$ and $0{\cdot}7$. There are nevertheless, as various effects of increasing Mach number become felt, considerable changes in the pressure distributions near the stall and in the nature of the stall. These effects are described in section 6 but it may be noted at this point that they combine to produce the minor variations in $C_{L\max}$ evident in Fig. 4a. There is a slight rise between M $M = 0{\cdot}3$ and $0{\cdot}4$, due probably to the increasing Reynolds number (*see* section 4.2 above). Beyond $M = 0{\cdot}4$ the effects of compressibility appear to become more important and $C_{L\max}$ begins to fall. This fall ceases between $M = 0{\cdot}45$ and $0{\cdot}5$ and is followed by a fairly sharp rise between $M = 0{\cdot}5$ and $0{\cdot}55$. With further increase of M, $C_{L\max}$ decreases again from the high value reached at $M = 0{\cdot}55$. These variations are typical of those observed for other low-drag sections of moderate t/c, the most significant difference between them and the corresponding variations for conventional sections of the same t/c being the interruption of the fall of $C_{L\max}$ by the fairly sharp rise, at Mach numbers between about $0{\cdot}5$ and $0{\cdot}6$, and the resulting higher values for Mach numbers above this.

Although for Mach numbers above $0{\cdot}7$ there is no peak in the C_L curve within the range of incidence covered, the maximum C_L attainable in trimmed flight would probably be limited by the rapid increase in nose-down pitching moment and may well fall below the value of about $1{\cdot}0$ measured at $0{\cdot}7$. The changes in flow pattern leading to the absence of a peak in the C_m curve and to the large negative pitching moments are discussed in section 6 and it is shown further that there are extensive boundary-layer separations which could cause buffeting in flight.

The curve of $C_{L\max}$ against M for the present tests is compared in Fig. 5a with those obtained for two very similar sections in the Ames 1-ft $\times$ $3\frac{1}{2}$-ft High-Speed Wind Tunnel[14] with almost the same Reynolds numbers, Fig. 2. The section characteristics are compared in Fig. 5c. The values of $C_{L\max}$ for both these N.A.C.A. sections are below those for the Goldstein section through most of the Mach number range, but there is a distinct similarity in the variation with Mach number. $C_{L\max}$ is somewhat higher for all three of these sections than the values predicted, for a section having the corresponding camber and thickness, from the results of Refs. 7 and 8 and indicated in Fig. 5a for $M = 0{\cdot}6$ and $0{\cdot}7$*.

6. *Detailed Observations.*—6.1. The detailed observations are discussed fairly fully with the object of bringing out the underlying causes of the variations in $C_{L\max}$ with Mach number for the present case and of illustrating certain flow phenomena and compressibility effects which occur at high incidences and which are thought to be of fairly general interest. Various effects become evident at different stages in the Mach number range, leading to successive changes in the way in which the forces develop with increasing incidence and in which the stall occurs. The general trend of the changes is introduced briefly in section 6.2 with reference to the pressure distributions near the stall for varying Mach number. The development of the pressure distributions and flow patterns with increasing incidence is then discussed in section 6.3 and 6.5 for each Mach number at which observations were made, with two particular features treated under separate headings in section 6.4 and 6.6. The main aspects are summarized and their significance remarked upon in section 7.

6.2. *General Trend of Changes with Increasing Mach Number.—Pressure Distributions near the stall.*—Fig. 6 shows on one scale a pressure distribution for each free-stream Mach number, the incidence in each case being chosen to be as near as possible to the incidence for maximum C_L. The minimum pressure coefficient on the upper surface is plotted against free-stream Mach number in Fig. 10 which also indicates the corresponding maximum local Mach numbers ; the dashed curves of $C_{p\min}$ give the variation for fixed incidences and the full curve the variation at the incidence for maximum C_L.

* (Note added in 1952). It has subsequently been shown in A.R.C. 14,802 that this discrepancy is only apparent and is due to the fact that the trailing-edge angles of these sections are considerably smaller than for any of the sections included in the tests of Refs. 7 and 8.

Low-speed distributions.—The pressure distribution for $M = 0{\cdot}3$ with very high peak suction, *i.e.*, low pressure coefficient, near the leading edge on the upper surface is typical for very high incidences and low speeds and the stall occurs because of the very large pressure recovery downstream of this peak. The distribution for $M = 0{\cdot}4$ is very similar but the local speed of sound is now exceeded, the peak suction corresponding to a local Mach number nearly $1{\cdot}2$.

Limiting of maximum local Mach number.—It is in the region of $M = 0{\cdot}4$ that an adverse effect of compressibility on $C_{L\,\max}$ first becomes evident. This is most probably caused by a limiting of the maximum local Mach number and the consequent increase in the minimum pressure coefficient with increasing free-stream Mach number. Thus the maximum local Mach number remains at about $1{\cdot}2$ for $M = 0{\cdot}4$ and $0{\cdot}45$, Fig. 10, with the result that $C_{p\,\min}$ falls considerably. This limit on the local supersonic Mach number is a well-known but not fully understood phenomenon. It is associated with a limit on the expansion that can occur in a local supersonic region of limited height.

Spread of supersonic region and rapid expansion to higher local Mach numbers.—The fall in $C_{L\,\max}$ is halted at a Mach number between $0{\cdot}45$ and $0{\cdot}5$ and there is a fairly sharp rise between $0{\cdot}5$ and $0{\cdot}55$. This is partly due to the spread of the low-pressure supersonic region which accompanies the rearward movement of the shock-wave on the upper surface and is very evident for $M = 0{\cdot}55$ (Fig. 6). It is also significant, however, that between $M = 0{\cdot}45$ and $0{\cdot}55$ there is a very marked decrease in the rate of rise of minimum pressure coefficient due to an increase in the maximum local Mach number to just over $1{\cdot}5$ at $M = 0{\cdot}55$ (Fig. 10). This high local Mach number is, moreover, reached very near the leading edge so that the supersonic expansion must be very rapid. It is suggested in section 6.4 with reference to the photographs obtained for $M = 0{\cdot}6$ that this rapid expansion is caused by an ' over-expansion ' around the bubble formed by a local separation or thickening of the boundary layer and further that this may help to explain the beneficial effect of a small nose-radius on $C_{L\,\max}$ at high speeds.

Further limiting of maximum local Mach number.—As the free-stream Mach number is increased further from $0{\cdot}55$ to $0{\cdot}65$ the maximum local Mach number is limited to about $1{\cdot}5$, Fig. 10, so that the rise in $C_{p\,\min}$ has again become rapid and $C_{L\,\max}$ again falls in spite of the continued spread of the supersonic region, Fig. 6. Between $M = 0{\cdot}65$ and $0{\cdot}7$, the highest Mach number for which there was a peak in the C_N curve, there is a continued rise in $C_{p\,\min}$ but no further spread of the supersonic region, and the fall in $C_{L\,\max}$ is accelerated.

The above changes in the pressure distributions near the nose on the upper surface are the most obvious effects of increasing free-stream Mach number and are probably one of the main factors contributing to the observed variations in $C_{L\,\max}$. There are however other factors involved.

Increased tendency to stall due to boundary-layer thickening.—It is clear, for example, from Fig. 6 that, as the Mach number is increased, the stall occurs with a reduced pressure recovery suggesting that some factor other than the magnitude of the pressure recovery is causing its onset. It is thought that this is the rapid boundary-layer thickening which, as shown in the further discussion in sections $6{\cdot}3$ and 6.5, occurs at the foot of the shock-wave on the upper surface and, for constant Mach numbers of about $0{\cdot}5$ and above, increases with increase of incidence in spite of little change in the shock strength and magnitude of the pressure recovery (*see*, for example, Figs. 16a and 16b). With a greater initial thickness, the turbulent boundary is likely to be able to withstand a smaller pressure recovery before separating, so that the increase in the thickening with increase of incidence introduces a tendency to stall with the same pressure recovery. This leads to the onset of the stall at a reduced incidence and in a region in which the magnitude of the pressure recovery is hardly changing with incidence. The consequent decrease in incidence for maximum C_L, Fig. 4b, must tend to reduce the value of $C_{L\,\max}$.

Pressures on lower surface.—The progressive decrease of the pressures over the lower surface, Fig. 6, which becomes more marked between $M = 0{\cdot}6$ and $0{\cdot}7$, must exert an adverse effect on $C_{L\,\max}$, continuous with increasing Mach number and accelerated at the higher Mach numbers.

It seems to be associated with a movement of the stagnation point towards the leading edge from a position at 0·03-chord on the lower surface at $M = 0{\cdot}3$. It is partly due to the decreasing incidence for maximum C_L, but not entirely so because similar trends are present for the pressure distributions for constant incidences, Figs. 7, 8 and 9.

Separation over the rear of the upper surfaces at incidences below the stall.—For the present case, there is a decrease with increasing Mach number in the extent of the turbulent boundary-layer separation, present at the rear of the upper surface before the stall, the separation being indicated by the roughly constant pressure in this region, Fig. 6. The effect of this change would be to increase $C_{L\,\max}$ slightly.

Changes leading to the absence of a peak in the C_N vs. α curves.—No pressure distributions for Mach numbers above 0·7 have been included in Fig. 6 because there are no peaks in the lift curves for these Mach numbers. The changes in flow pattern which lead to the absence of the peak are discussed in section 6.5 for $M = 0{\cdot}75$. The main feature is that the pressure distribution on the upper surface retains a form similar to that for $M = 0{\cdot}7$ in Fig. 6 up to the highest incidence of the test without any collapse of the low-pressure supersonic flow.

Supersonic expansion at the trailing edge on the lower surface.—The pressure distributions in Fig. 6 show that the pressure at the trailing edge approaches the sonic pressure as the free-stream Mach number is increased; it falls below the sonic value at Mach numbers above 0·7. This is accompanied by the occurrence of a supersonic expansion at the trailing edge on the lower surface. The expansion appears to reduce the adverse effect which the separation on the upper surface exerts on the rate of increase of circulation with increase of incidence; this is discussed in section 6.6.

6.3. *Development of pressure distributions and flow patterns with increasing incidence; $M = 0{\cdot}3$ to $0{\cdot}55$.*—$M = 0{\cdot}3$. The high peak suctions near the leading edge on the upper surface develop with increasing incidence, Fig. 11, and pressure rises over the lower surface. Above $\alpha = 6{\cdot}5$ deg, the flattening out of the pressures over the rear of the upper surface suggests that the separation in this region (*see* Appendix III) spreads forward gradually and reaches a position at about mid-chord for $\alpha = 13{\cdot}5$ deg, the incidence for maximum C_N.

At higher incidences the separation moves rapidly to near the leading edge, causing the collapse of the peak suction, and the pressures on the lower surface cease to rise; the combined effects of these changes are a drop in C_N and a rapid increase in nose-down C_m.

$M = 0{\cdot}4$. The local speed of sound is exceeded very near the nose on the upper surfaces for incidences greater than 10·5 deg, Fig. 12a, and a maximum local Mach number of nearly 1·2 is reached at 12·5 deg, the incidence for maximum C_N. In other respects the development of the pressure distributions resembles that described above for $M = 0{\cdot}3$. Observations of separation with oil on the surface were obtained over a wider range of incidence for this particular Mach number; the results (Table 4) confirm that the reversed flow spreads forward to about 0·55-chord for 12·5 deg. At 13·5 deg the oil was almost stationary over the rest of the surface as though separation was about to move right forward to the leading edge.

The direct-shadow photographs, Fig. 12b, show that there are very small shock-waves near the leading edge on the upper surface for 12·5 deg, followed by a turbulent boundary layer which is initially fairly thin but which thickens rapidly. The shock-waves are even smaller for 13·5 deg but the turbulent boundary layer is very thick right from the leading edge. For higher incidences there are no shock-waves, the peak suction having fallen to below the sonic value; the stalled boundary layer thickens extremely rapidly, however.

$M = 0{\cdot}45$. The limiting of the maximum local Mach number to about 1·2 and the consequent increase in minimum pressure coefficient is reflected in the reduced rate at which the peak develops with increasing incidence between 8·5 deg and 12·5 deg, Fig. 13. The rise in C_N is maintained by the slight reduction in pressure over the rest of the upper surface and the increase in pressure over most of the lower surface.

The development of the separation over the rear of the upper surface below the stall and of the stall itself appear from the pressure distributions to be very similar to that for $M = 0{\cdot}3$ and $0{\cdot}4$.

$M = 0{\cdot}5$. The local speed of sound is first exceeded at $8{\cdot}5$ deg and there are shock-waves present, Fig. 14b, very near the leading edge on the upper surface for this and higher incidences. The height of the supersonic region is very small but there are nevertheless some well-formed, complex patterns shown more clearly in the enlargements in Fig. 14c for $8{\cdot}5$ deg and $10{\cdot}5$ deg*. Fuller descriptions are given in Appendix II.

As far as can be ascertained from the pressure points available, there is little change in the peak suction between $\alpha = 9{\cdot}5$ deg and $\alpha = 11{\cdot}5$ deg, Fig. 14a, the increasing C_N again being maintained by the favourable trends on the rest of the upper surface and on the lower surface. There is also practically no change in the magnitude of the pressure recovery between $9{\cdot}5$ deg and $11{\cdot}5$ deg but, in spite of this, the stall occurs just above $11{\cdot}5$ deg. The photographs show, however, that the thickening of the boundary layer at the foot of the shock-wave on the upper surface increases considerably, there being a very marked change between $10{\cdot}5$ deg and $11{\cdot}5$ deg although the shock patterns are the same and the normal shocks are of about the same strength at the surface. As discussed in section 6.2 above, this increase in thickening would introduce a greater tendency to stall and it is thought that it does in fact lead to the onset of the stall in this case and is responsible for the reduction in the incidence for maximum C_L, Fig. 4b.

The photographs for $\alpha = 12{\cdot}5$ deg and above suggest that the turbulent separation has spread to near the leading edge ; this is confirmed by the pressure distributions. The shock-waves have become very diffuse for these incidences.

The pressure distributions indicate that the extent of the separation at the rear of the upper surface, before the stall, is limited to about the rear $0{\cdot}3$-chord compared with $0{\cdot}4$ to $0{\cdot}5$-chord for the lower Mach numbers.

$M = 0{\cdot}55$. The pressure distributions for this Mach number, Fig. 15a, show the rearward spread of the low pressure supersonic region between $8{\cdot}5$ deg.and $10{\cdot}5$ deg incidence and the increase in the maximum local Mach number to $1{\cdot}5$, these being the changes which are largely responsible for the halt in the tendency for $C_{L\,\max}$ to fall with increasing free-stream Mach number and the fairly abrupt rise between $M = 0{\cdot}5$ and $0{\cdot}55$.

The expansion to the local Mach number of $1{\cdot}5$ is extremely rapid and occurs within the first $0{\cdot}02$-chord. The flow phenomenon which is thought to cause this rapid expansion is discussed in the next section.

The upper surface pressures indicate that at $10{\cdot}5$ deg, the incidence for maximum C_N, the extent of the separation is the rear $0{\cdot}3$-chord and that it spreads rapidly towards the leading edge with further increase of incidence.

6.4. *The Rapid Supersonic Expansion near the Leading Edge on the Upper Surface.*—The very rapid expansion to local supersonic Mach numbers of about $1{\cdot}5$ near the leading edge on the upper surface has been remarked upon by Cooper and Korycinski[10] who noted a marked difference in this respect between an NACA 66 series section and a conventional section which, because of the further forward maximum thickness, had a larger nose radius. They suggest that, since the rapid expansion is associated with a small nose radius, it may be caused by a flow phenomenon similar to that observed for very sharp-nosed aerofoils[19], namely a separated laminar boundary on the nose, which is deflected back towards the surface by a supersonic expansion (*see* Fig. i). There is a compression shock associated with the further change in direction as the layer flows along the surface, but the net result could be a greater expansion than would occur in the absence of the separation. The occurrence of this phenomenon is well-established for sharp-nosed aerofoils in high-subsonic[19] and supersonic flow[20] and for square-nosed objects in supersonic flow[21].

* The apparent distortion of the nose of the profile on the direct-shadow photographs is due to the deflection of the light outwards caused by the rapid density changes near the stagnation point.

FIG. i.

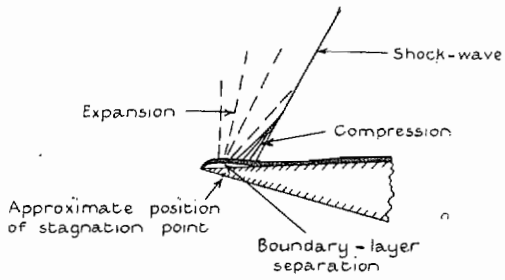

Unfortunately, in the present tests no photographs were taken for $M = 0{\cdot}55$, but the rapid expansion occurs for higher Mach numbers also, for example, $M = 0{\cdot}6$, Fig. 16a. On the direct-shadow photographs taken at $M = 0{\cdot}6$, Fig. 16b, there are small waves very near the nose on the upper surface for $\alpha = 8{\cdot}5$ deg to $10{\cdot}5$ deg. It is thought that these waves are associated with flow phenomenon similar to that described above and that the essential features are sketched as in Fig. ii. At this position, and especially for fairly low free-stream Mach numbers, the height of the local supersonic region is small and the expansion and shock-waves consequently extend only a short distance above the surface. The reason for the occurrence of the second, weaker shock-wave is not clear, but it has been observed elsewhere, *e.g.*, Ref. 21.

FIG. ii.

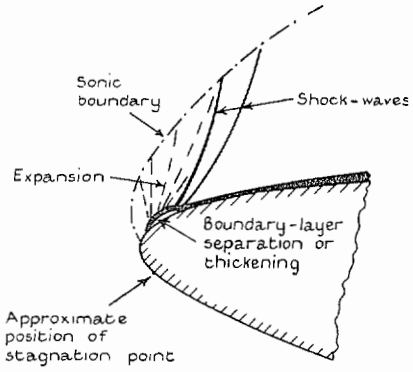

It is significant that, for $M = 0{\cdot}6$, these waves are first evident at $8{\cdot}5$ deg, the angle for which the rapid expansion is first shown by the pressure distribution, Fig. 16a. This is also the case for higher Mach numbers and the position is summarized in Table 3 for those examples where both photographs and pressure distributions are available. The chordwise position of the point at which the local Mach number of $1{\cdot}4$ is reached has been taken as an arbitrary guide to the rapidity of the expansion and is indicated in columns (1), the values being given in fractions of the chord from the leading edge. The presence of the small waves on the photographs is recorded by an asterisk in columns (2); where no waves were present the word 'none' is inserted. Dashes indicate the case for which no photographs are available.

TABLE 3

α (deg)	$M = 0{\cdot}6$		$M = 0{\cdot}65$		$M = 0{\cdot}7$		$M = 0{\cdot}75$		$M = 0{\cdot}775$	
	(1)	(2)	(1)	(2)	(1)	(2)	(1)	(2)	(1)	(2)
6·5	—	—	—	—	—	—	0·34	None	—	—
8·5	0·05	*	0·08	*(slight)	0·16	None	0·2	None	0·2	None
9·5	0·01	*	$0{\cdot}03_5$	*	0·07	*(slight)	—	—	0·15	None
10·5	0·01	*	$0{\cdot}02_5$	*	0·05	*	0·07	*(v. slight)	0·09	*(v. slight)
11·5	$0{\cdot}01_5$	*	—	—	—	—	0·05	*(slight)	—	—
12·5	—	—	0·02	*	0·03	*	—	—	—	—
13·5	—	—	—	—	—	—	0·02	*	—	—
14·5	—	—	—	—	0·01	*	—	—	—	—

The waves are clearly defined for all cases in which $M_L = 1{\cdot}4$ is reached within the first $0{\cdot}05$ chord, *i.e.*, for a very rapid expansion. There is evidence of very slight waves where $M_L = 1{\cdot}4$ is reached between $0{\cdot}05$-chord and about $0{\cdot}09$-chord, but none at all when the expansion is more gradual than this.

This confirms that the rapid expansion at the leading edge, shown by the surface pressure distributions, is probably due to the typical flow pattern of an over-expansion, around the bubble formed by a local separation or thickening of the boundary layer, followed by a compression shock. It is reasonable to assume that this is also the case for $M = 0{\cdot}55$ and that it accounts for the increase in maximum local Mach number evident in Fig. 10 for this free-stream Mach number* and, at least in part, for the increase in $C_{L\,\max}$.

Cooper and Korycinski[10] show that the rapid expansion is the main cause of a higher $C_{L\,\max}$ for a low-drag section than on a conventional section of the same thickness. The present results add weight to their suggested explanation for the beneficial effect of a small nose radius on $C_{L\,\max}$ at high speeds.

There was close agreement between tunnel and flight tests for the low-drag section described in Ref. 10, particularly with regard to the sharp rise in $C_{L\,\max}$ starting at about $M = 0{\cdot}5$ which was shown by the pressure distributions obtained in the tunnel tests to be due to the rapid expansion to an increased local supersonic Mach number. Similar agreement between tunnel and flight[9] was also obtained for one of the sections used in the Ames High-Speed Tunnel tests[12]. This suggests that rapid supersonic expansions similar to those described above occur in flight also, on sections with small leading-edge radii.

6.5. *Development of Pressure Distributions and Flow Patterns with Increasing Incidence; $M = 0{\cdot}6$ to $0{\cdot}775$.*—$M = 0{\cdot}6$. The pressure distributions for $M = 0{\cdot}6$, Fig. 16a, show a more marked rearward spread of the local supersonic region as the incidence is increased from $6{\cdot}5$ deg to $9{\cdot}5$ deg, which, combined with the rising pressure over the lower surface, is sufficient to give a rising C_N in spite of very little increase in the peak suction. The expansion to local Mach numbers of about $1{\cdot}4$ to $1{\cdot}5$ is very rapid for incidences above $8{\cdot}5$ deg, but since there is no further increase in the maximum value, this being just over $1{\cdot}5$ at $10{\cdot}5$ deg, there is an increase in $C_{p\,\min}$ which is partly responsible for the renewed fall in $C_{L\,\max}$ from the high value at $M = 0{\cdot}55$.

The incidence for maximum C_L has fallen to just below $10{\cdot}5$ deg compared with $13{\cdot}5$ deg for low Mach numbers. The direct-shadow photographs, Fig. 16b, again show a marked increase in the thickening of the turbulent boundary layer at the foot of the shock between $8{\cdot}5$ deg and $10{\cdot}5$ deg, which most probably causes the stall and occurs in spite of a very similar shock pattern and practically no change in the strength of the wave at the surface or in the magnitude of the pressure recovery.

With increase in Mach number from $0{\cdot}5$ the shock-waves, Fig. 16b, have moved rearwards along the surface and increased in height above the surface corresponding to the growth of the supersonic region rearwards and outwards. At $6{\cdot}5$ deg there is a single upstream-inclined shock-wave, reflected from the surface at about $0{\cdot}1$-chord as an expansion, followed by a normal shock at about $0{\cdot}15$-chord. This shock-wave pattern is described more fully in Appendix II. The observations of oil on the surface, Table 4, indicate a local separation of the laminar boundary layer in the region of the reflection with re-attachment after transition to turbulent flow.

The shock-waves at $8{\cdot}5$ deg, $9{\cdot}5$ deg and $10{\cdot}5$ deg are single, near-normal waves occurring at the rear end of the supersonic region at about $0{\cdot}2$-chord. If the explanation, given in section 6.4 above, of the small waves very near the nose on the photographs in Fig. 16b is correct, it implies the presence of a local separation at this position which was not observed in the tests with oil (Table 4), possibly because it extends for only a very short distance (*see* section 2.2). Following this separation, the boundary layer must re-attach as a laminar layer because it remains

* It is very probable that the very high local peak Mach numbers of $1{\cdot}6$ and $1{\cdot}7$ observed for other aerofoils with small leading-edge radii[10, 25] were associated with a similar flow pattern.

laminar until just upstream of the main shock-wave, as shown by the presence of the bright line separated from the image of the aerofoil[18]. This type of re-attachment can presumably occur by virtue of the fact that the layer is deflected towards the surface by the supersonic expansion. The oil tests, Table 4, show that there is a second local separation starting at about 0·15-chord with re-attachment at about 0·2-chord, which in this case occurs in the normal way after transition to turbulent flow.

Boundary-layer thickening commences from the leading edge for incidences above 10·5 deg and the shock-waves become diffuse. The turbulent separation has moved to near the leading edge at 12·5 deg (Table 4).

The turbulent separation on the upper surface below the stall is limited to the rear 0·2-chord, confirming the tendency observed at $M = 0{\cdot}5$ and 0·55 for the extent of this to be reduced with increasing free-stream Mach number.

$M = 0{\cdot}65$. Although there is a further spread of the low-pressure supersonic region, Fig. 17a, the maximum local Mach number is limited to about 1·46, so that the C_p are higher than those for $M = 0{\cdot}6$, Figs. 6 and 10, and $C_{L\,\max}$ continues to fall. Other factors contributing to this fall are the increased rate of fall in pressure over the lower surface, evident in Fig. 6, and the further reduction in incidence for maximum C_L. The photographs, Fig. 17b, show that the boundary-layer thickening at the foot of the shock-wave is more marked at 9·5 deg than at 8·5 deg and could lead to the occurrence of the stall between 9·5 deg and 10·5 deg.

The boundary layer is again laminar until just upstream of the main shock-wave for 8·5 deg and 9·5 deg, Fig. 17b, and there is a local separation of this laminar layer at about 0·27-chord with re-attachment at about 0·3-chord. It is noticeable that the thickening of the re-attached turbulent layer starts upstream of the normal shock-wave. This would tend to give a gradual compression upstream of the main compression and is probably partly responsible for the gradual rise in surface pressures in this region, Fig. 17a.

The shock-wave and commencement of the boundary-layer thickening have moved towards the leading edge for 10·5 deg and are even nearer the leading edge at 12·5 deg. The pressures indicate that there is a separation over most of the surface at 12·5 deg. The photograph for 12·5 deg and the pressure distribution for 16·5 deg suggest that there are spanwise variations in the stalled flow.

The oil tests, Table 4, show that the turbulent separation at the rear of the upper surface below the stall, observed for lower Mach numbers, is not present. This is confirmed by the absence of any flattening out of the surface pressures in this region.

$M = 0{\cdot}7$. There is an extensive region of local supersonic flow on the upper surface even for comparatively small positive angles, Fig. 18a, and which at 4·5 deg stretches from near the leading edge to beyond 0·5-chord. Unlike the behaviour at lower speeds, the extent of this region decreases with increasing incidence even below the stall, the increasing lift being maintained, but at a reduced rate, by increasing local supersonic Mach numbers between $\alpha =$ 4·5 deg and 6·5 deg, a more rapid expansion at the leading edge, reduced pressures over the rear half of the upper surface between $\alpha = 6{\cdot}5$ deg and 9·5 deg and a continuing rise in pressure over most of the lower surface up to 9·5 deg. The increase in nose-down pitching moment with increase of incidence above 6·5 deg is due mainly to the reduction in pressure over the rear half of the upper surface. The reduction in the extent of the supersonic region with increasing incidence is accompanied by a movement forwards of the shock-wave, Fig. 18b, and of the commencement of the rapid boundary-layer thickening.

$\partial C_N/\partial\alpha$ falls roughly to zero at $\alpha = 9{\cdot}5$ deg and the value of C_L at this incidence has been taken as $C_{L\,\max}$ because, in spite of a further rise in C_N, the boundary layer is stalled and probably separated over much of the chord for higher incidences.

As discussed in section 6.2 and illustrated by Figs. 6 and 10, the factors leading to the increased rate of fall in the value of $C_{L\,max}$ between $M = 0{\cdot}65$ and $0{\cdot}7$ are the continued rise in $C_{p\,mid}$ accompanied by the restriction in the extent of the local supersonic region at the incidence for maximum C_L, the reduction in pressure on the lower surface and the further, slight reduction in the incidence for maximum C_L. The photographs suggest again that the onset of the stall is influenced by the increased boundary-layer thickening at the foot of the shock-wave as the aerofoil incidence is increased.

The further rise in C_N for incidences above $10{\cdot}5$ deg is due to the beginning of changes in the flow pattern which become more apparent at higher Mach numbers and lead to the absence of the peak in the C_N versus α curves. These will be discussed later for $M = 0{\cdot}75$. There is a tendency for the flow to adhere over more of the upper surface and for the shock-wave to move rearwards and become more inclined. There is also a continued rise in pressure on the lower surface in spite of the separation on the upper surface. The changes in the positions of the shock-wave and boundary-layer thickening lead to the spanwise variations evident in the photographs of Fig. 18b. The effect of these on the accuracy of the results is discussed above in section 4.1.

$M = 0{\cdot}75$; *incidences up to* $8{\cdot}5$ *deg.* There is an extensive supersonic region on the upper surface even at $-1{\cdot}5$ deg, Fig. 19a, and with increasing incidence the local Mach numbers in this region at first increase. The position of the main recompression remains at about $0{\cdot}5$ to $0{\cdot}6$-chord for incidences up to $4{\cdot}5$ deg and then moves forward to about $0{\cdot}4$-chord for $8{\cdot}5$ deg. The maximum local Mach number is limited to about $1{\cdot}43$. The increasing C_N is maintained between $4{\cdot}5$ deg and $8{\cdot}5$ deg by decreasing pressure over the rest of the upper surface, particularly near the leading edge and trailing edge, and the increasing pressure over the forward part of the lower surface. The pitching-moment coefficient falls between $4{\cdot}5$ deg and $8{\cdot}5$ deg incidence, due chiefly to the reduced pressures over the rear of the upper surface.

The shock-wave, Fig. 19b, changes from a near-normal wave at about $0{\cdot}6$-chord for $\alpha = -1{\cdot}5$ deg to a wave inclined backwards and forked near its foot, which is at about $0{\cdot}4$-chord, for $\alpha = 8{\cdot}5$ deg. The rapid boundary-layer thickening moves forward with the foot of the shock-wave and becomes more pronounced as the incidence is increased. A considerable increase in the height of the shock-wave above the surface is also evident, indicating a large growth in the height of the supersonic region.

$M = 0{\cdot}75$; *incidences above* $8{\cdot}5$ *deg.* For incidences above $8{\cdot}5$ deg the supersonic region extends right to the tunnel wall and the observations for these incidences, shown in Fig. 20, were obtained under this condition. Although the effect of tunnel constraint is therefore probably fairly large, it is thought that these results may be of some value in illustrating qualitatively the development of the flow pattern which leads to the continuing increase in C_N instead of the usual turning over in the C_N vs. α curve and which was just beginning at $M = 0{\cdot}7$ (*see* above). It should be noted that this continued rise in C_N, Fig. 3, is accompanied by a rapid increase in nose-down pitching moment and that it is therefore doubtful whether this régime would be attainable in trimmed flight.

Instead of moving forward to the leading edge as at speeds below $M = 0{\cdot}7$, the shock-wave remains at about mid-chord, Fig. 20, with an adhered laminar boundary layer back at its foot. The wave becomes more inclined with the result that the pressure rise through it is reduced and the flow at the edge of the very thick, separated boundary layer remains supersonic. There is a second, near-normal shock which meets the wake behind the trailing edge and which moves off the field of the photograph at $13{\cdot}5$ deg. The two waves join at a height of about one-chord above the surface. A further feature to note on the photographs is the occurrence of a centred supersonic expansion at the trailing edge on the lower surface.

The most important difference between the pressure distributions and those for Mach numbers below $0{\cdot}7$ is the maintained low pressure supersonic region on the front half of the upper surface,

the collapse of which at the lower Mach numbers causes the drop in C_N. The factors contributing to the continued rise in C_N are the reduction in pressure over the rear half of the upper surface, the slight reduction also over the front half of this surface, and the increase in pressure over the whole of the lower surface. The first of these is associated with the reduced rise through the inclined shock-wave and the development of the boundary-layer separation. The second is probably due to the increased height of the supersonic region which would tend to reduce the influence of the surrounding subsonic region on the flow at the surface ; it is in this respect that the effect of the supersonic region spreading to the tunnel wall would be most serious. The continued increase in pressure over the lower surface in spite of the extensive separation on the upper surface is contrary to trends at lower Mach numbers. It is thought to be connected with the occurrence of the supersonic expansions at the trailing edge and is discussed in section 6.6.

$M = 0{\cdot}775$. The pressure distributions for incidences up to $6{\cdot}5$ deg are given in Fig. 21. For incidences of $8{\cdot}5$ deg and above, the local supersonic region on the upper surface stretches to the tunnel walls and the results obtained under this condition are shown in Fig. 22.

The development of the flow with increasing incidence is very similar to that described for $M = 0{\cdot}75$ except that the changes in the shock-wave pattern occur at an earlier incidence. There is again a continuing rise in C_N, Fig. 3, but again a rapidly increasing nose-down pitching moment, in this instance over the whole incidence range.

More of the field behind the trailing edge was obtained in the photographs for $9{\cdot}5$ deg and $10{\cdot}5$ deg and these show more clearly the rear branch of the shock-wave on the upper surface and a shock-wave which occurs behind the trailing edge on the lower surface. Evidently the supersonic expansion at the trailing edge gives a region of supersonic flow stretching quite a distance below the surface and terminated by a fairly strong shock-wave as sketched in Fig. iii.

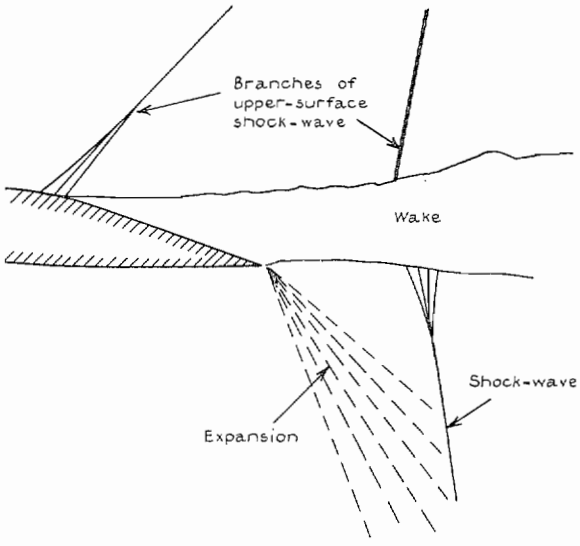

FIG. iii.

6.6. *The Occurrence and Effects of Supersonic Expansions at the Trailing Edge.*—Preston[26] has shown for incompressible flow that, in order to satisfy the condition of zero net vorticity being shed into the wake, the velocities at the edges of the upper-surface and lower-surface boundary-layers must be nearly equal at the trailing edge. This relation will be modified for the case with shock-waves since the flow is no longer isentropic or irrotational, but for the following qualitative explanation it will be good enough here to assume that the static pressures at the edges of the boundary-layers at the trailing edge must be closely related. Thus any large decrease in pressure at the edge of the upper-surface boundary-layer at the trailing edge, due to boundary-layer thickening or separation, must be accompanied by a similar decrease at the edge of the boundary layer on the lower surface at this position. This will normally affect the circulation and to some extent the pressures over the rest of the lower surface,

For the pressure distributions of the present tests, it is noticeable that the trailing-edge pressure hole records a value continuous with the distribution over the rear of the upper surface, *e.g.*, Fig. 14a. The pressures recorded at the surface of the aerofoil are approximately equal to the static pressures at the edge of the boundary-layer and therefore the pressure at the trailing hole must correspond fairly closely to the static pressure at the edge of the boundary-layer on the upper surface.

The fall in pressure over the rear of the upper surface, including the trailing edge, which always accompanies marked boundary-layer thickening or separation is shown clearly for $M = 0{\cdot}5$, Fig. 14a, for example. When this occurs there is a rapid expansion on the lower surface between about 0·9-chord and the trailing edge, corresponding to an acceleration at the edge of the lower-surface boundary-layer. The pressure over the rest of the lower surface is also affected, however, for most cases. This is shown in Fig. 26 for $M = 0{\cdot}5$, which is typical for all Mach numbers below 0·7, the pressure coefficients for fixed chordwise positions being plotted against incidence. The fall in pressure at the trailing edge begins at about 4·5 deg and causes a slight decrease in the rate of rise in pressure over the rest of the lower surface ; this must be at least partly responsible for the drop in $\partial C_N/\partial\alpha$ below the stall. A more rapid fall in trailing-edge pressure begins at the stall. The pressure over the lower surface then ceases to rise and begins to fall ; this must contribute to the fall in C_N.

With increasing incidence at $M = 0{\cdot}75$ there is a continuous fall in pressure at the trailing edge, Fig. 26, due to the changes in the shock-waves and the development of the separation on the upper surface. This at first affects the whole of the lower surface, there being a falling pressure over the rear, shown by the curve for $x/c = 0{\cdot}727$, and a decreasing rate of rise over the rest of the surface. Above about 8·5 deg, however, these tendencies are reversed, the pressures now rising at $x/c = 0{\cdot}727$ and the rate of increase over the rest of the surface being accelerated ; $\partial C_N/\partial\alpha$ also increases.

The pressure at the trailing edge falls below the sonic value* at 8·20 deg. Reference to Figs. 19a and 20a shows that the expansion at the rear of the lower surface becomes noticeably more rapid with further increase in incidence and at 13·5 deg it occurs almost entirely between the last pressure hole at 0·945-chord and the trailing edge ; it also increases considerably in magnitude. That part of the expansion from the sonic pressure down to the pressure recorded by the trailing edge hole occurs in a centred supersonic expansion which shows up on the direct-shadow photographs†, Fig. 20b. This is even more clear in the photographs for $M = 0{\cdot}775$, Fig. 22b.

It is significant that the first occurrence of this supersonic expansion coincides with the reversal in the effect which the falling pressure on the upper surface exerts on the rate of rise of pressure on the lower surface. It seems that in the presence of this expansion, the rest of the lower surface is no longer affected. In other words, the adverse effect which the development of the separation over the rear of the upper surface exerts on the rate of increase of circulation is considerably reduced.

There are, Fig. 27, similar increases in the rate of rise of pressure on the lower surface when the trailing-edge pressure falls below the sonic value at $M = 0{\cdot}7$ and $0{\cdot}775$, the incidences for which this occurs being 12·7 deg and 6 deg respectively, and similar increases in $\partial C_N/\partial\alpha$.

---

* The value of the sonic pressure calculated for isentropic flow is slightly in error on the upper surface, but it should, however, be fairly accurate for conditions on the lower surface where there were no shock-waves or boundary-layer separations.

† Schlieren photographs are more sensitive to gradual density changes than those obtained by the direct-shadow method and those in Fig. 25, for example, show the more gradual expansion in this region for some cases, the expansion showing up as a black area.

7. *Concluding Discussion.*—7.1. *On the Usefulness of the Method.*—The stall was covered for uncorrected free-stream Mach numbers up to 0·7 in the present case and results obtained over a useful range of incidence for still higher Mach numbers at which the usual peak did not occur in the C_N vs. α curve. The maximum load on the model produced no signs of failure.

The choking Mach number for a given incidence should be higher for the models of the systematic series since the maximum thickness is smaller. Those models of the series which are of 10 per cent t/c will be supported in the same way and the strength limitations will be the same. A new method of support will be used for the models of 6 per cent t/c which will be equally strong. Thus the same, if not a slightly greater range should be available.

The limitations on the accuracy of the results due to tunnel interference and low Reynolds number are not likely to detract from the main purpose of this type of experiment which is to study qualitatively the explanation of effects from the detailed observations and flow photographs. The most serious of these limitations is likely to arise from the spanwise variations which are most marked in the small critical range of Mach number where the type of lift curve changes from a curve with the usual stall to that for which the stall is delayed.

7.2. *On the Results for the Present Section.*—The variation in $C_{L\,\max}$ for the Goldstein section agrees well with that observed on similar sections in an American tunnel which was somewhat larger relative to the chord. This variation can be explained qualitatively with reference to the shock-wave photographs and pressure distributions. The most important feature of the variation of the pitching moment at high incidence is the rapid increase in nose-down moment, which occurs even at Mach numbers above 0·7 where there is no stall in the lift curves. These rapid changes in moment may of themselves limit the range of C_L available in flight.

The detailed results, including the pressure distributions, photographs and observations of boundary-layer separation, illustrate certain known compressibility effects at high incidences and reveal other features, some of which may be of general significance.

Thus the limit on the local supersonic Mach number on the upper surface is clearly shown with the consequent increase in the pressure coefficients on this surface, *e.g.*, Fig. 10, which contributes to the general tendency for $C_{L\,\max}$ to fall with increasing free-stream Mach number. It is significant that, for the present case, a reversal of this tendency between $M = 0{\cdot}5$ and $0{\cdot}55$ is accompanied by an increase in the maximum local Mach number from just over $1{\cdot}2$ to just over $1{\cdot}5$. Above $M = 0{\cdot}55$ there is no further increase in the local Mach number and $C_{L\,\max}$ again falls. At $M = 0{\cdot}55$ and above, the local expansion to about $M_L = 1{\cdot}5$ occurs very rapidly and is associated with the appearance of small waves near the nose of the aerofoil on the direct-shadow photographs; the pattern of these waves is similar to those observed elsewhere due to an over-expansion around the bubble formed by a local laminar separation. This tends to confirm the suggestion made by Cooper and Korycinski[10] and adds weight to their argument that this rapid expansion may be the main cause of the beneficial effect of reduced nose radius on $C_{L\,\max}$ at high Mach numbers.

A further feature which becomes evident as the free-stream Mach number is increased, and which is thought to be of general importance, is the increasing tendency to stall due to the influence of the rapid thickening of the turbulent boundary layer at the foot of the shock-wave on the upper surface. The extent of the thickening increases with incidence in spite of little change in the strength of the shock at its foot. This increase is apparently sufficient to bring about the stall at a lower incidence than at low speeds and in a region where the magnitude of the pressure recovery is hardly changing. For the present section this feature is apparent for Mach numbers between 0·5 and 0·7.

The flow changes which are associated with the change in the type of lift curve to the curve without a stall are illustrated qualitatively. This change has been observed in many other tests for Mach numbers above about 0·75, depending on the section, but there have been few

other detailed observations in this region. Although there is still considerable thickening of the turbulent boundary layer at the foot of the shock-wave on the upper surface (*see*, for example, Fig. 22b) and, at the higher incidences, separation at this point, this separation and shock-wave do not move forward to the leading edge with increase of incidence as at lower Mach numbers. Instead, the boundary layer remains adhered back to about 0·5-chord and the low-pressure supersonic flow persists. The height of the supersonic region grows and the front branch of the shock-wave becomes inclined with a smaller pressure recovery through it ; the separation prevents any further recovery upstream of the trailing edge. The resulting low pressure over the rear half of the upper surface helps to augment the C_L but causes large nose-down pitching moments in this régime. In the present case, these flow changes are also accompanied by the occurrence of a centred supersonic expansion at the trailing edge on the lower surface when the pressure at the trailing edge, falling with increasing incidence due to the separation on the upper surface, has dropped to below the sonic value. This leads to a reduction in the adverse effect which the separation on the upper surface exerts on the circulation. This may be important, but the precise significance is difficult to assess in the present case because of the increased effect of tunnel constraint under these conditions.

The occurrence of a turbulent separation over the rear of the upper surface at incidences below the stall caused non-linearities in the lift curves and a considerable falling off in lift-curve slope in some cases. This separation disappeared for a small range of moderate Mach numbers (0·65 to 0·7) due to the rearward spread of the shock-wave and the consequent reduction in length of the turbulent boundary layer. This is likely to be of limited application, however, since it may be peculiar to this type of section and low Reynolds numbers.

7.3. *On Suggestions for Further Experiments.*—A better understanding of the importance of these factors would result from further tests of this type, especially on a systematic series of aerofoils. Moreover, tests on the series suggested by Beavan and Hills[1] would bring out the underlying causes of the known beneficial effects of certain section parameters and may enable a fuller use to be made of these effects. For example, the favourable effects of reduced nose radius on $C_{L\,\max}$ at high speeds are opposite to the trends at low speeds. Also, the favourable effect of camber does not extend through the whole C_L range and at moderate C_L symmetrical sections usually show a better high speed performance. A fuller understanding of these conflicting tendencies may lead to improvements in the design for good all-round performance.

It is also important to obtain further measurements of pitching-moment coefficients and to compare the variation of these for a series of sections because it may be less favourable on some sections than on others.

The C_L obtainable in flight is also sometimes limited by buffeting before an actual stall would be expected, particularly at Mach numbers above 0·7. It is clear from the present results that there is often, at these speeds, a marked separation which produces no sign of a maximum in the lift curve but which could cause severe buffeting. It has been suggested by Holder that, if any further tests of this nature are made, an attempt should be made to detect buffeting in the wake by means of some simple device such as a vane free to oscillate with rapid changes of downwash.

It is difficult to investigate factors affecting the stalling of an aerofoil by any means except on an aerofoil itself since they are intimately bound up with the circulation and flow around the whole aerofoil. It may however be possible to study some specific aspects by special experiments on curved plates or on a tunnel wall. For example, preliminary studies on the problem of the boundary-layer thickening at the foot of a shock-wave and how it is affected by changes in curvature and inclination to the main stream could be made in an experiment of the type developed by Ackeret, Feldmann and Rott[16]. It would probably still be necessary to extend this to experiments on aerofoils in order to determine just how this thickening causes the onset of the stall.

An experiment could probably be devised to explore in detail the 'over-expansion', or local supersonic expansion around a local laminar separation, which is thought to occur very near the nose of aerofoils with small leading-edge radii, even at comparatively low free-stream Mach numbers. Thus if a forward-facing suction slot were inserted in the wall of a wind tunnel with the rear lip protruding, as sketched in Fig. 31, the flow around this lip should be similar to that around the leading edge of an aerofoil at incidence. It should be possible to control the position of the stagnation point either by adjusting the suction quantity or the amount by which the lip protrudes into the stream. Lips having different radii and shapes could be inserted.

8. *Acknowledgment.*—The authors wish to acknowledge the assistance of Miss N. A. Bumstead in the experiment described in this report.

REFERENCES

No.	*Author*	*Title, etc.*
1	J. A. Beavan and R. Hills	$C_{L\,max}$ of aerofoil sections at high subsonic Mach number. A.R.C. 11,102. December, 1947. (Unpublished.)
2	J. A. Beavan	Programme of high-subsonic tests on aerofoils in the N.P.L. 20-in. × 8-in. wind tunnel. A.R.C. 12,233. March, 1949. (Unpublished.)
3	H. H. Pearcey and J. A. Beavan ..	Force and pressure coefficients up to Mach number 0·87 on the Goldstein roof-top section 1442/1547. R. & M. 2346. April, 1946.
4	D. W. Holder	The High-Speed Laboratory of the Aerodynamics Division, N.P.L. R. & M. 2560. 1947.
5	C. N. H. Lock and J. A. Beavan ..	Tunnel interference at compressibility speeds using the flexible walls of the Rectangular High-Speed Tunnel. R. & M. 2005. September, 1944.
6	L. K. Loftin and W. J. Bursnall ..	The effects of variation in Reynolds number between $3{\cdot}0 \times 10^6$ and $25{\cdot}0 \times 10^6$ upon the aerodynamic characteristics of a number of N.A.C.A. 6-series airfoil sections. N.A.C.A. Tech. Note 1773. December, 1948.
7	J. A. Beavan, R. F. Sargent and P. M. Burrows.	Measurements of maximum lift on 19 aerofoil sections at high Mach number. R & M. 2678, January, 1948.
8	R. J. North and P. M. Burrows ..	Measurements of the maximum lift of a further 7 aerofoils at high Mach number: R. & M. 2678. January, 1948 (Addendum).
9	J. R. Spreiter and P. J. Steffen ..	Effect of Mach and Reynolds numbers on maximum lift coefficient. N.A.C.A. Tech. Note 1044. March, 1946.
10	M. Cooper and P. F. Korycinski ..	The effects of compressibility on the lift, pressure and load characteristics of a tapered wing of N.A.C.A. 66-series airfoil sections. N.A.C.A. Tech. Note 1697. October, 1948.
11	G. C. Furlong and J. E. Fitzpatrick ..	Effects of Mach number and Reynolds number of the maximum lift coefficient of a wing of N.A.C.A. 230-series airfoil sections. N.A.C.A. Tech. Note 1299. May, 1947.

REFERENCES—*continued*

12	F. E. West and J. M. Hallissy	Effects of compressibility on normal-force, pressure and load characteristics of a tapered wing of N.A.C.A. 66-series airfoil sections with split flaps. N.A.C.A. Tech. Note 1759. December, 1948.
13	E. N. Jacobs and A. Sherman	Airfoil section characteristics as affected by variations of the Reynolds number. N.A.C.A. Report 586. 1937.
14	D. J. Graham, G. E. Nitzberg and R. N. Olson.	A systematic investigation of pressure distributions at high speeds over five representative N.A.C.A. low-drag and conventional airfoil sections. N.A.C.A. Report 832. 1945.
15	H. E. Cleary	Effects of compressibility on maximum lift coefficients for six propeller airfoils. N.A.C.A. A.C.R. L4L21a. January, 1945.
16	J. Ackeret, F. Feldmann and N. Rott..	Investigations on compression shocks and boundary layers in fast moving gases. (Institut für Aerodynamik, ETH, Zürich, No. 10. 1946.) (Translated by I. M. Davidson and G. Korbacher.) A.R.C. 10,044. September, 1946.
17	H. W. Liepmann	Investigations of the interaction between shock-waves and boundary layer in transonic flow. *J.Aero.Sci.*, Vol. 13, p. 623. 1946.
18	H. H. Pearcey	The indication of boundary-layer transition on aerofoils in the N.P.L. 20-in. × 8-in. High-Speed Wind Tunnel. Current Paper 10. December, 1948.
19	W. F. Lindsey, B. N. Daley and M. D. Humphreys.	The flow and force characteristics of supersonic airfoils at high subsonic speeds. N.A.C.A. Tech. Note 1211. 1947.
20	J. Valensi and F. W. Pruden	Some observations on sharp-nosed profiles at supersonic speed. R. & M. 2482. May, 1947.
21	D. W. Holder, R. C. Tomlinson and E. W. E. Rogers.	Preliminary experiments on blunt-nosed plates in supersonic airstreams. A.R.C. 12,418. June, 1949.
22	R. C. Pankhurst and H. H. Pearcey ..	Camber derivatives and two-dimensional tunnel interference at maximum lift. Current Paper 28. April, 1950.
23	R. A. Mendelsohn and J. F. Polhamus	Effect of the tunnel-wall boundary layer on test results of a wing protruding from a tunnel wall. N.A.C.A. Tech. Note 1244. April, 1947.
24	K. W. Todd, Metropolitan-Vickers Electrical Co. Ltd.	An experimental study of three-dimensional high-speed air conditions in a cascade of axial-flow compressor blades. R. & M. 2792. October, 1949.
25	E. W. E. Rogers and C. White	Force and pressure measurements up to Mach number 0·88 on a 10 per cent thick modified N.A.C.A. 16-series propeller section. A.R.C. 11,114. December, 1947. (Unpublished.)
26	J. H. Preston	The calculation of lift taking account of the boundary layer. R. & M. 2725. November, 1949.
27	J. S. Thompson	Present methods of applying blockage corrections in a closed rectangular high-speed wind tunnel. A.R.C. 11,385. January, 1948. (Unpublished.)
28	D. W. Holder and R. J. North	An oscillatory flow resulting from the interaction of shock-waves with the boundary layer on a rigid aerofoil. A.R.C. 12,400. June, 1949. (To be published.)
29	A. E. von Doenhoff and N. Tetervin ..	Investigation of the variation of lift coefficient with Reynolds number at a moderate angle of attack on a low-drag airfoil. N.A.C.A. Confidential Bulletin. A.R.C. 6570. November, 1942.

APPENDIX I

Formulae used to Calculate the Corrections for Tunnel Constraint; Two-dimensional case.—These formulae are well known but since some have been used in slightly different forms from those usually employed, they are all listed below.

1. *Corrections for Effect of Curvature of Flow,* i.e., *' Lift Effect.'*—The corrections for effective change in camber and effective change in incidence are often grouped together in correcting C_L and C_m This leads to difficulties at high incidences near the stall and it therefore seems better to keep them separate as follows:

(*a*) Correction on C_L due to effective change in camber:

$$\Delta C_L = -\frac{\pi^2}{48\beta^2}\left(\frac{c}{2h}\right)^2 C_L$$

(*b*) Correction on C_m due to effective change in camber:

$$\Delta C_m = \frac{\pi^2}{192\beta^2}\left(\frac{c}{2h}\right)^2 C_L$$

(*c*) Correction on α due to effective change in incidences of stream:

$$\Delta\alpha = \frac{\pi}{96\beta^2}\left(\frac{c}{2h}\right)^2 (C_L + 4C_m) \text{ radians.}$$

These formulae are obtained from Ref. 22.

2. *Corrections for ' Blockage Effect '*

(*a*) Corrections on force coefficients:

$$\delta C = -(2 - M^2)(\varepsilon_1 + \varepsilon_2)C.$$

(*b*) Correction on Mach number:

$$\delta M = (1 + \tfrac{1}{5}M^2)(\varepsilon_1 + \varepsilon_2)M.$$

These are given in Ref. 27

3. *Total Corrections*

$$C_L' = C_L + \Delta C_L + \delta C_L$$
$$C_m' = C_m + \Delta C_m + \delta C_m$$
$$\alpha' = \alpha + \Delta\alpha$$
$$M' = M + \delta M.$$

Notation

C_L, C_m, C_D, α, M	Uncorrected force coefficients, incidence and free-stream Mach number
C_L', C_m', α', M'	Corrected ditto.
ΔC_L, ΔC_m, $\Delta\alpha$	Corrections due to curvature of flow
δC_L, δC_m, δM	Corrections due to blockage
β^2	$1 - M^2$
c	Aerofoil chord
$2h$	Tunnel height
ε_1	$= \dfrac{0{\cdot}045\pi \times \text{cross-sectional area of aerofoil profile}}{\beta^2 h^2}$ (*i.e.*, component of blockage due to solidity of model)
ε_2	$= \dfrac{cC_D}{8\beta^2 h}$ (*i.e.*, component due to wake blockage)

APPENDIX II

Interesting Shock-Wave Formations

1. $M = 0{\cdot}5$, $\alpha = 8{\cdot}5$ deg *and* $10{\cdot}5$ *deg.*—The direct-shadow photographs of these formations are reproduced in Figs. 14b and 14c. The sequence at $8{\cdot}5$ deg appears to be as sketched in Fig. iv*, starting with a small expansion region followed by a shock-wave which is inclined upstream slightly to the local direction of flow and which in turn is followed by a further expansion. There are then six more small shock-waves, each, except the last, being followed by an expansion. The conditions at the foot at each except the last of the shock-waves resembles the ' free-jet ' reflection such as often occurs at a separated laminar boundary layer; the presence of a local separation followed by re-attachment was confirmed in this case in the oil tests (Table 4). The pressure rise through each shock-wave is counteracted by the drop through the expansion which follows it and, although there may be a periodic variation at a short distance above the surface, the pressure at the surface is likely to be nearly constant, probably rising slowly. An abrupt rise would be expected through the final shock. There are insufficient pressure points to show the details of this in the pressure distributions of Fig. 14a.

FIG. iv.

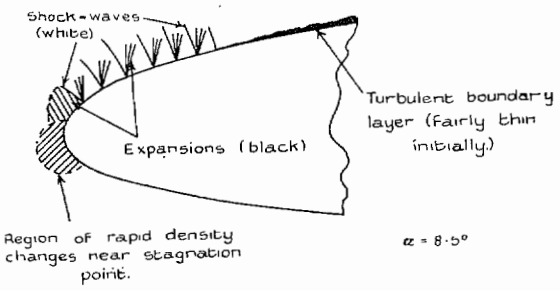

Similar shock-wave patterns have been observed under certain conditions by Liepmann[17] and by Holder and North[28] in the larger local supersonic regions existing at about mid-chord for aerofoils at low incidences and slightly higher free-stream Mach numbers.

At $\alpha = 10{\cdot}5$ deg, the repeated shocks have consolidated into a single ' lambda shock ', *i.e.*, a forked shock the main branch of which is inclined upstream to the local direction of flow. The lambda shock is followed by an expansion and a near-normal shock as sketched in Fig. v. This pattern is similar to that observed by Ackeret, Feldmann and Rott[16] for a part of the Mach number range covered in their tests on a curved plate.

FIG. v.

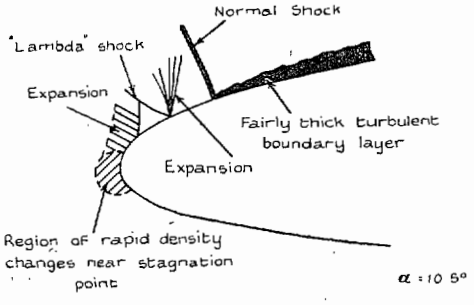

Although there were no oil tests at $10{\cdot}5$ deg incidence, the reflection of the main branch of the lambda wave suggests that there was again a local laminar separation.

* A shock-wave shows up in a direct-shadow image as a bright line downstream of a less obvious black line, and a supersonic expansion as a black area with often a more diffuse bright area upstream. The difference in sharpness occurs because a shock-wave is much more abrupt than an expansion and also because the optical convergence is more marked for a shock-wave.

2. $M = 0{\cdot}6$; $\alpha = 6{\cdot}5$ *deg.*—The pattern for $M = 0{\cdot}6$, $\alpha = 6{\cdot}5$ deg, sketched in Fig. vi shows an interesting further development. The single upstream-inclined wave at about 0·15-chord replaces the lambda wave present for $M = 0{\cdot}5$, $\alpha = 10{\cdot}5$ deg, and closely resembles in shape the rear branch of that wave. The pattern is otherwise very similar to that for $M = 0{\cdot}5$, $\alpha = 10{\cdot}5$ deg. In fact, apart from the increased height of the waves due to the growth of the supersonic region above the surface, the only essential difference amounts to the absence of the front branch of the lambda wave. It is thought that this difference arises because of the increased Reynolds number of the laminar boundary layer at the position of the shock which in this case has moved further aft along the surface. It is suggested that the front branch of the lambda wave occurs at the point of separation of the laminar boundary layer for $M = 0{\cdot}5$, $\alpha = 10{\cdot}5$ deg, but that for $M = 0{\cdot}6$, $\alpha = 6{\cdot}5$ deg, the compression at the point of separation is more gradual and does not form an abrupt shock ; the presence of a local separation in this region was confirmed by the observations of oil on the surface (Table 4).

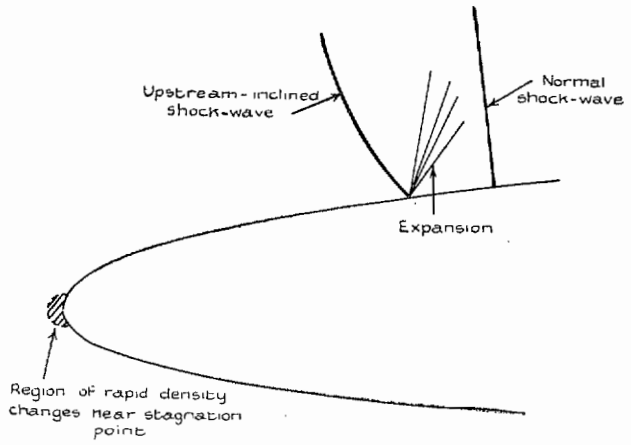

FIG. vi.

This shock-wave pattern at $M = 0{\cdot}6$, $\alpha = 6{\cdot}5$ deg, is similar to a formation observed and described in detail by Liepmann[17].

APPENDIX III

Boundary-Layer Effects at Incidences Below the Stall

1. *Correlation between Lift-Curve Slope and Trailing-Edge Pressure.*—The curves of Figs. 28 and 29 have been included to show the correlation which exists between the lift-curve slope and the pressure coefficients over the rear of the upper surface and particularly at the trailing edge. $\partial C_N/\partial\alpha$ is plotted against α for each of several Mach numbers together with the corresponding pressure coefficients for the fixed chordwise positions 0·725, 0·8, 0·9-chord on the upper surface and for the trailing edge, i.e., $x/c = 1{\cdot}0$.

Referring first to Fig. 28, $\partial C_N/\partial\alpha$ begins to fall off at quite a low incidence, varying from about 4·5 deg ($C_L = 0{\cdot}6$) at $M = 0{\cdot}3$ to about 1·5 deg ($C_L = 0{\cdot}35$) at $M = 0{\cdot}7$. In all cases the pressure coefficient at the trailing edge begins to fall at almost the same incidence. The drag results in Ref. 3 show that these incidences also correspond very closely to the limits of the low-drag range.

The pressure at the trailing edge is very nearly equal to the pressure at the edge of the boundary layer on the upper surface at this position. The fall in its value, *i.e.*, an increase in velocity at the edge of the boundary layer, is, for Mach numbers below 0·6 at any rate, presumably caused by the increasing thickness of the upper surface boundary layer at this position as the transition point moves forward, the forward movement starting at the limit of the low-drag range. The effect of this thickening on the circulation is described by Preston in Ref. 26. He shows that in order to satisfy the condition of zero net vorticity being shed into the wake the static pressures at the edges of the boundary layers at the trailing edge must be approximately equal for the two surfaces. Thus if there is a decrease in pressure at this point on the upper surface there must be a corresponding decrease on the lower surface and therefore a decrease in circulation. This would be expected to produce just such a falling-off in lift-curve slope as is observed.

The observations with oil on the surface, Table 4, showed that for Mach numbers of 0·6 and below, the turbulent boundary layer first separates over the rear of the upper surface at an angle between 4·5 deg and 6·5 deg. The building up of this separation causes a continuing fall in trailing-edge pressure and lift-curve slope. The observations of separation were continued up to the stall for $M = 0{\cdot}4$ and 0·6 only. For these two cases the approximate extent of the turbulent separation is indicated in Fig. 28.

At $M = 0{\cdot}4$, the separation affects the pressures for the other chordwise positions shown, increasing the pressure at $x/c = 0{\cdot}725$ and 0·8 and decreasing it at $x/c = 0{\cdot}9$ and 1·0. This leads to a flattening out in the pressure distribution in this region and at 10 deg the pressure is nearly constant from $x/c = 0{\cdot}725$ to the trailing edge. Between 10 deg and 12 deg there is a halt in the fall of the trailing-edge pressure, due probably to a halt in the build-up of separation, and a slight increase in $\partial C_N/\partial\alpha$. The pressure coefficients and lift-curve slope behave very similarly at $M = 0{\cdot}5$ except that the halt in the build-up of separation and the increase in $\partial C_N/\partial\alpha$ are more marked. This feature is absent at $M = 0{\cdot}3$.

At $M = 0{\cdot}6$ the extent of the turbulent separation diminishes between about 7 deg and 10 deg with the result that there is a reversal in the flattening out of the pressures and an earlier increase in lift-curve slope. This reduction in the extent of separation occurs when the shock-wave moves back over the upper surface ; it is discussed in section 2 below.

The oil indicated that for $M = 0{\cdot}65$ and 0·7 there is no turbulent separation over the rear of the upper surface at 6·5 deg and 8·5 deg and this is confirmed by the absence of any flattening out in the pressures. The trailing-edge pressure still falls in a similar manner, however, presumably due to the continued boundary-layer thickening ; $\partial C_N/\partial\alpha$ falls continuously, there being no reversal as at lower Mach numbers and consequently no kinks in the lift curves.

For $M = 0{\cdot}75$ and 0·775 the trailing-edge pressure is falling over the whole incidence range. The lift-curve slope at first falls but begins to rise again at an incidence corresponding almost exactly to that at which the sonic pressure is first reached at the trailing edge. This aspect is discussed in section 6.6 and is associated with the occurrence of a Prandtl-Meyer expansion at the trailing edge. For these Mach numbers, the lift-curve slope does not fall to zero within the range of incidence tested.

2. *Extent and Causes of Turbulent Separation over the Rear of the Upper Surface.*—Observations with oil on the surface were made at $\alpha = 4{\cdot}5$ deg, 6·5 deg and 8·5 deg through the Mach number range. These indicate, Table 4, reversed flow on the upper surface, from the trailing edge forward to about 0·8-chord at 6·5 deg and to about 0·7-chord at 8·5 deg for all Mach numbers up to about 0·6*. The observations were continued up to the stall at $M = 0{\cdot}4$ and 0·6 only, but in other cases a fairly good idea of the development of the separation is obtained from the surface pressures (*see* above).

* The schlieren photographs in Fig. 14d for $M = 0{\cdot}5$, $\alpha = 8{\cdot}5$ deg and 10·5 deg also show this turbulent separation, the dead-air region showing up as a region of normal illumination between the light separated boundary layer and the black aerofoil.

As the Mach number is increased there is a tendency for this development below the stall to be restricted and in a small range of Mach number between 0·6 and 0·7 there is no turbulent separation until immediately before the stall.

The effects of this separation on lift-curve slope have already been described ; further comments will be confined to the causes of the separation and for its absence at Mach numbers between 0·6 and 0·7.

The occurrence of separation under these conditions may be peculiar to this type of section or to the low Reynolds numbers. It is of interest that the same kind of variation in lift-curve slope was present[14] for the two N.A.C.A. ' low-drag ' sections mentioned in section 5.1 above whereas the lift curves for three ' conventional ' sections, of the same thickness and tested under the same conditions, were straight up to an incidence very near the stall over the whole of the low and medium range of Mach number.

This greater tendency towards separation on the part of the low-drag sections may be due to the concavity of the surface in this region. It may also be influenced by the bubble, formed by the separation of the laminar boundary layer and its re-attachment as a turbulent layer, which often occurs near the comparatively sharp leading edges of these sections at angles outside of the low-drag range and leads to an increase in the initial thickness of the turbulent boundary-layer. Thus, in Ref. 29, von Doenhoff and Tetervin noted that a similar falling-off in lift-curve slope at low speeds became less marked with increasing Reynolds number. This was attributed to a reduction in the extent of the laminar separation near the leading edge and the resulting decrease in the initial thickness of the turbulent boundary layer, which was then able to withstand a greater pressure recovery before separating.

The trend for the development of the separation below the stall to be restricted as the free-stream Mach number is increased above about 0·5 and the absence of the separation at $M = 0{\cdot}65$ and 0·7 are no doubt related effects and due to the development of the shock-waves. This is illustrated by the oil observations for varying Mach number at the fixed incidences of 6·5 deg and 8·5 deg, Figs. 23 and 24 respectively. At 6·5 deg, Fig. 23a, the shock-wave moves back from about 0·1-chord at $M = 0{\cdot}6$ to about 0·5-chord at $M = 0{\cdot}7$ and a local laminar separation followed by transition and re-attachment, occurring just ahead of the wave, moves back with it. The separation over the rear disappears at Mach number between 0·625 and 0·65 and is absent until a Mach number of just over 0·7 is reached. For $M = 0{\cdot}725$ and 0·75 there is again a separation over the rear which now spreads forward to the shock-wave at about 0·5-chord, there being no re-attachment after the laminar separation. There are similar effects at 8·5 deg, the rear separation disappearing at Mach number between 0·6 and 0·625. The observations were not continued above $M = 0{\cdot}7$ for this incidence and the Mach number was not reached at which this separation again occurred.

Some condition connected with the rearward movement of the shock-waves is evidently more favourable between $M = 0{\cdot}6$ and 0·7 than for lower Mach numbers for the adherence of the turbulent boundary layer over the rear of the upper surface. This cannot be the initial thickness of the layer as it thickens very rapidly at the foot of the shock-wave immediately after formation and, in fact, it has been suggested above that, for incidences only slightly higher than these, the very considerable initial thickening may lead to the stall and more general separation. The adverse pressure gradients are moreover still quite severe, but it is thought that the delay in the formation of the turbulent layer is important with the consequent reduction in the distance over which it is subjected to these gradients.

For other tests[8, 10, 14] where separations of this type were present at low Mach numbers there are indications that these also disappeared for moderate Mach numbers between about 0·6 and 0·75 in that the lift curves became straighter and that there was less flattening out of the surface pressures over the rear.

TABLE 4

Approximate Chordwise Positions, as Indicated by Oil, of Boundary-Layer Separations on the Upper Surface

M	α											
	4·5 deg		6·5 deg		8·5 deg		10·5 deg		12·5 deg		13·5 deg	
	Local laminar separation	Turbulent separation	Local laminar separation	Turbulent separation	Local laminar separation	Turbulent separation	Local laminar separation	Turbulent separation	Local laminar separation	Turbulent separation	Local laminar separation	Turbulent separation
0·3	—	—	—	0·9→1·0	0·05	0·75→1·0						
0·4	—	—	—	0·8→1·0	0·05	0·75→1·0	0·05	0·7→1·0	Very near nose	0·55→1·0	Very near nose	About to spread over whole surface
0·45	—	—	—	0·88→1·0	0·05	0·7→1·0						
0·5	—	—	—	0·85→1·0	0·06	0·7→1·0						
0·55	—	—	0·8	0·8→1·0	0·05→1·0	0·7→1·0						
0·575	—	0·9→1·0										
0·6	—	—	0·07→0·13	0·8→1·0	0·15→0·20	0·8—1·0	0·10—0·15	0·9→1·0	Whole surface from 0·1→1·0			
0·625	—	—	0·22	0·8→1·0	0·20→0·25	—						
0·65	—	—	0·27→0·3	—	0·25→0·30	—						
0·7	about 0·5	—	0·45→0·5	—	0·28→0·30	—						
0·725			0·45→1·0			—						
0·75	0·51→1·0		0·45→1·0									

A dash thus — indicates that there was no separation.

A blank space indicates that no observation was made.

TABLE 5

Summary of the Successive Changes in Flow with Increasing Free-Stream Mach Number

Free-stream Mach number	Incidence at which sonic speed is first reached on upper surface (deg)	Maximum local Mach number observed on upper surface	$C_{L\,max}$	Incidence for maximum C_L (deg)	Most important change with each increase in free-stream Mach number
0·3 (Fig. 11)	—	0·84	1·056	13·5	Fairly typical 'low-speed' stall for section of this type and thickness
0·4 (Figs. 12a and 12b)	10·7	1·17 (at 12·5 deg)	1·093	12·5	First free-stream M at which local sonic speed is exceeded.
0·45 (Fig. 13)	8·5	1·21 (at 12·5 deg)	1·049	12·7	First free-stream M at which limitation on local supersonic M on the upper surface becomes evident.
0·5 (Figs. 14a and 14b)	6·9	1·33 (at 10·5 deg)	1·047	11·8	First free-stream M at which the boundary-layer thickening at the foot of the shock-wave on the upper surface noticeably influences onset of stall.
0·55 (Fig. 15)	5·3	1·52 (at 10·5 deg)	1·161	10·2	Rearward spread of local supersonic region on the upper surface first evident. Also, first free-stream M at which very rapid expansion near nose and increased local M's occur. Fairly abrupt rise in $C_{L\,max}$ with M.
0·6 (Figs. 16a and 16b)	4·2	1·52 (at 10·5 deg)	1·104	10·1	Association between rapid expansion near leading edge and local supersonic 'over-expansion' confirmed. Local M now limited to 1·5 and so further increase in $C_{p\,min}$ with increasing free-stream M. Effect on stall of increasing boundary-layer thickening also confirmed.
0·65 (Figs. 17a and 17b)	2·8	1·46 (at 9·5 deg)	1·066	9·7	Absence of separation over rear of upper surface at incidences below stall. Increased rate of fall of pressure on the lower surface with increasing M first evident.
0·7 (Figs. 18a and 18b)	— 1·4	1·47 (at 14·5 deg, *i.e.*, above stall)	0·932	9·5	Supersonic region on front of upper surface through whole incidence range. Changes in flow pattern which lead to the absence of peak in lift curve becoming evident at high incidences. Considerable spanwise variations at high incidences.
0·75 (Figs. 19a, 19b and 20a)	$< 1·5$	—	No maximum in curve	—	Changes evident in flow pattern which lead to the absence of the peak in the lift curve. Separation and rapid increase in nose-down pitching moment in spite of this absence of the peak.
0·775 (Figs. 21a, 22a and 22b)	$< 1·5$	—	No maximum in curve	—	Above changes confirmed.

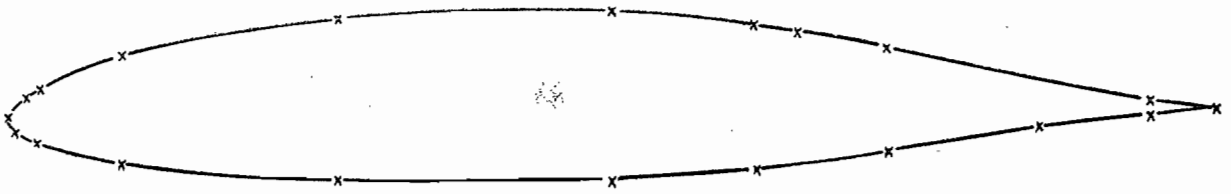

× Position of pressure holes.

Ordinates (chords)

x/c	0·005	0·010	0·015	0·025	0·05	0·1	0·15	0·2	0·25	0·3	0·35	0·4	0·45	0·5	0·55	0·6	0·65	0·7	0·75	0·8	0·85	0·9	0·95	1·0	Leading Edge Radius
y/c Upper	0·0113 5	0·0162	0·0200	0·0260	0·0371	0·0520	0·0625	0·0702	0·0761	0·0803	0·0830	0·0845	0·0849	0·0852	0·0804	0·0755	0·0676	0·0581	0·0476	0·0367	0·0260	0·0158	0·0069	0	$\rho/c = 0·0114_5$
y/c Lower	0·0100 5	0·0139	0·0167	0·0212	0·0287	0·0382	0·0445	0·0488	0·0519	0·0543	0·0562	0·0555	0·0550	0·0538	0·0515	0·0480	0·0425	0·0360	0·0291	0·0220	0·0151	0·0088	0·0036	0	

FIG. 1. Goldstein roof top aerofoil 1442/1547 : 5-in. chord.

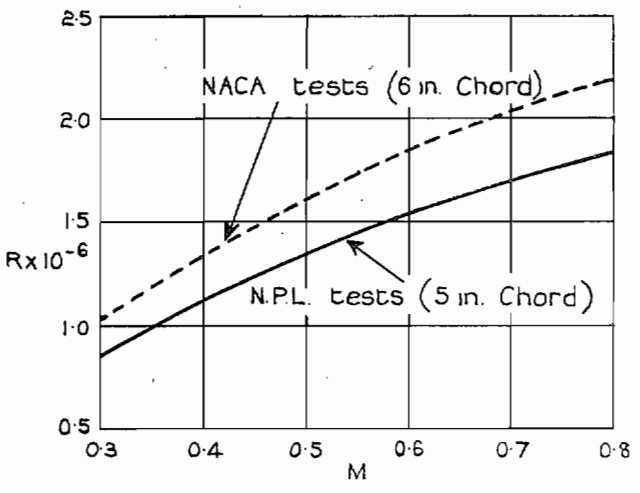

FIG. 2. Variation of Reynolds number with free-stream Mach number.

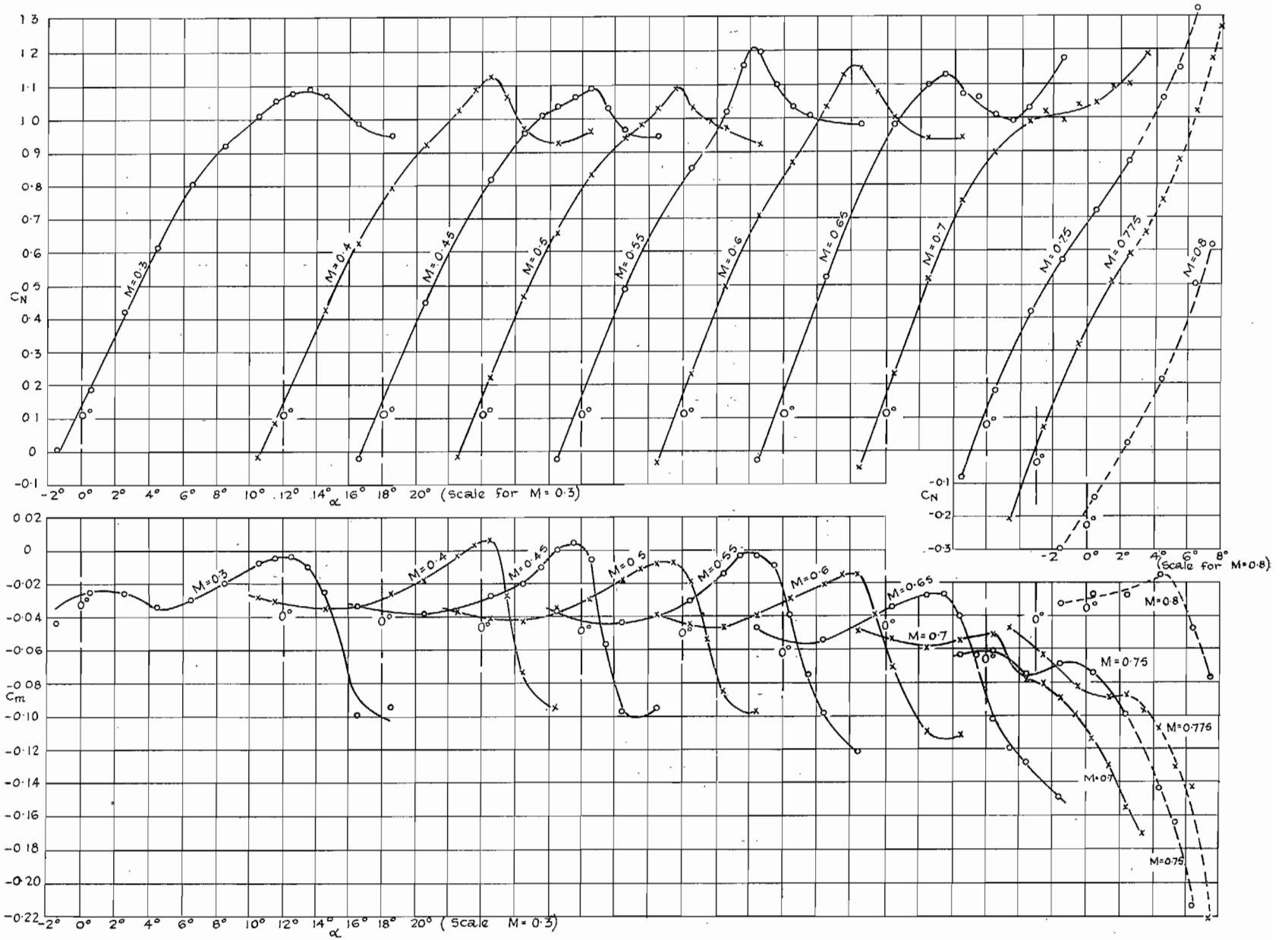

FIG. 3. C_N and C_m plotted as functions of incidence (α) for constant Mach numbers (M).

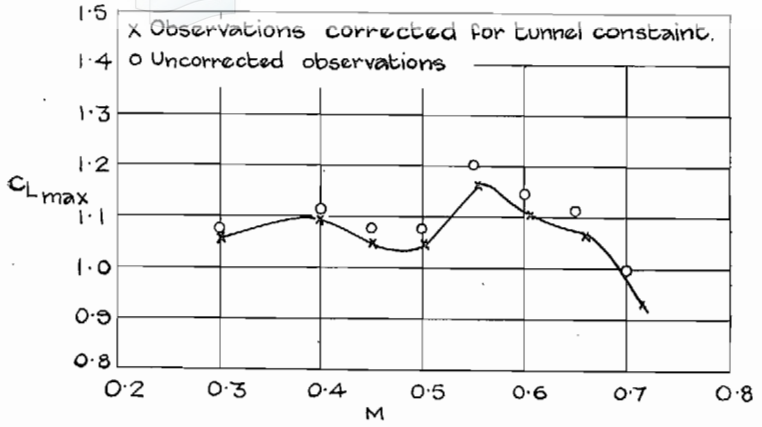

FIG. 4a. Variation of $C_{L\,max}$ with Mach number.

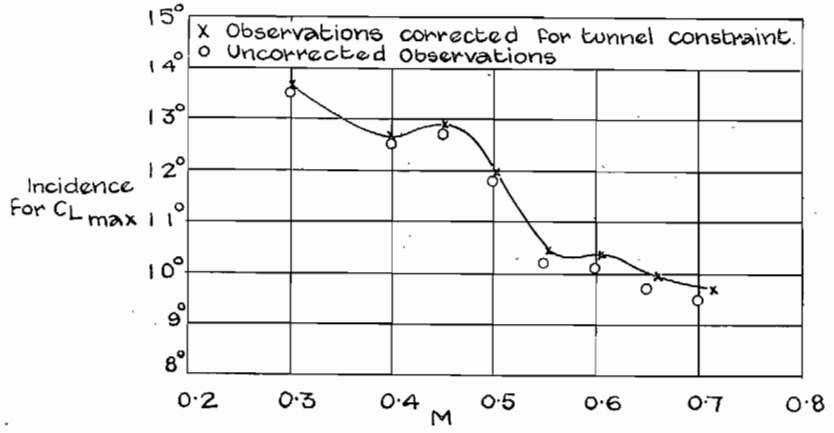

FIG. 4b. Variation of incidence for maximum lift coefficient with Mach number.

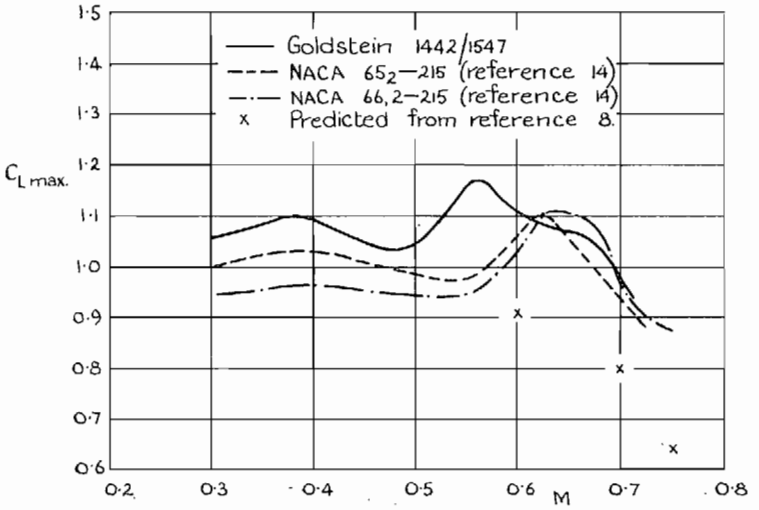

(a) $C_{L\,max.}$

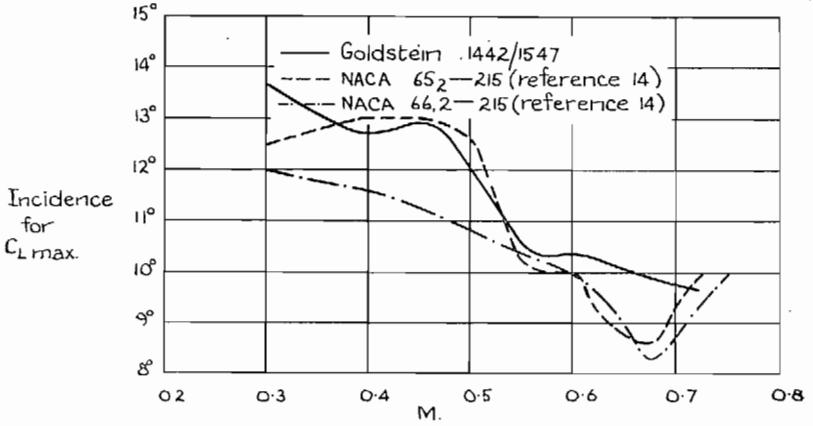

(b.). Incidence for Maximum C_L.

FIGS. 5a and 5b. Comparisons with tests elsewhere on similar sections.

Section	Thickness		Camber		Leading-edge radius
	Maximum	Position of maximum	Maximum	Position of maximum	
Goldstein Roof-Top	0·14 chord	0·42 chord	0·015 chord	0·47 chord	0·0114 chord
NACA 65_2-215	0·15 chord	0·41 chord	0·015 chord	0·44 chord	0·0150 chord
NACA 66_1,2-215 (a=0·6)	0·15 chord	0·46 chord	0·015 chord	0·475 chord	0·0138 chord

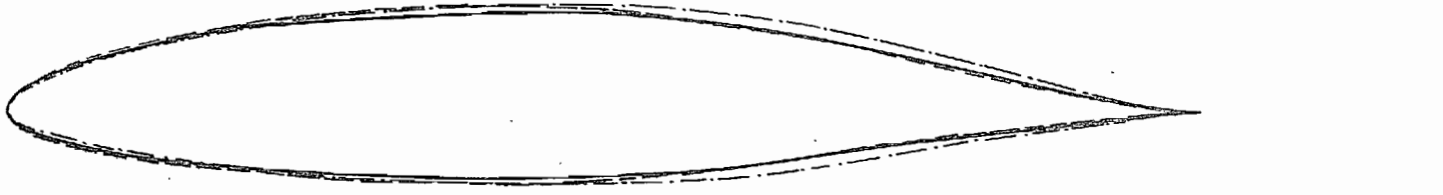

(c) Details of Sections.

FIG. 5c. Comparisons with tests elsewhere on similar sections.

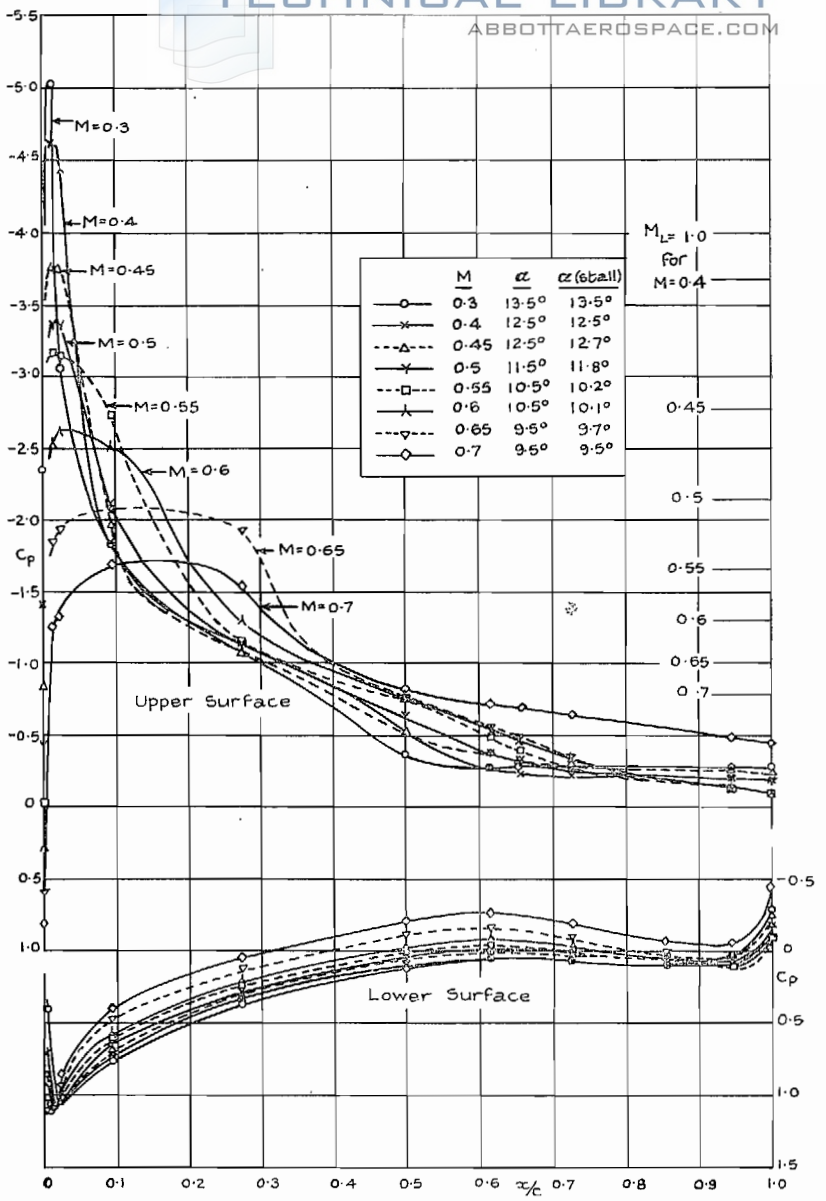

FIG. 6. Pressure distributions for various uncorrected Mach numbers at an angle very near that for maximum C_L in each case.

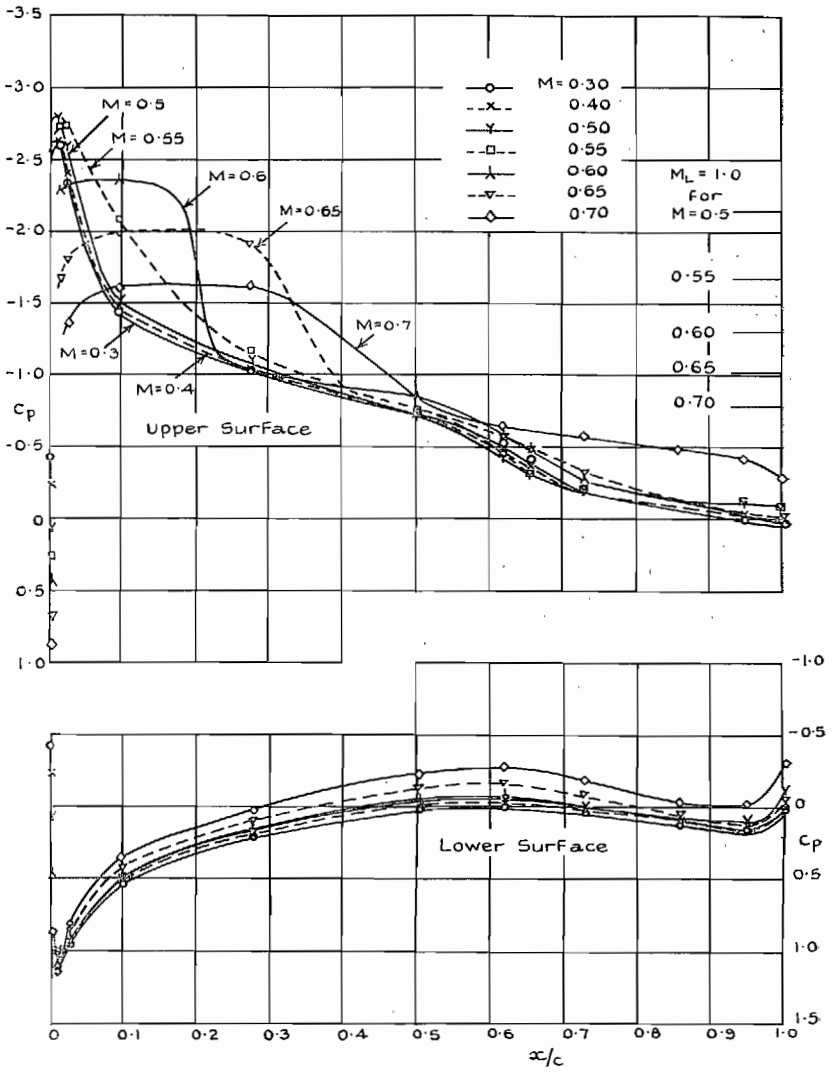

FIG. 7. Pressure distributions for various Mach numbers at 8·5 deg incidence.

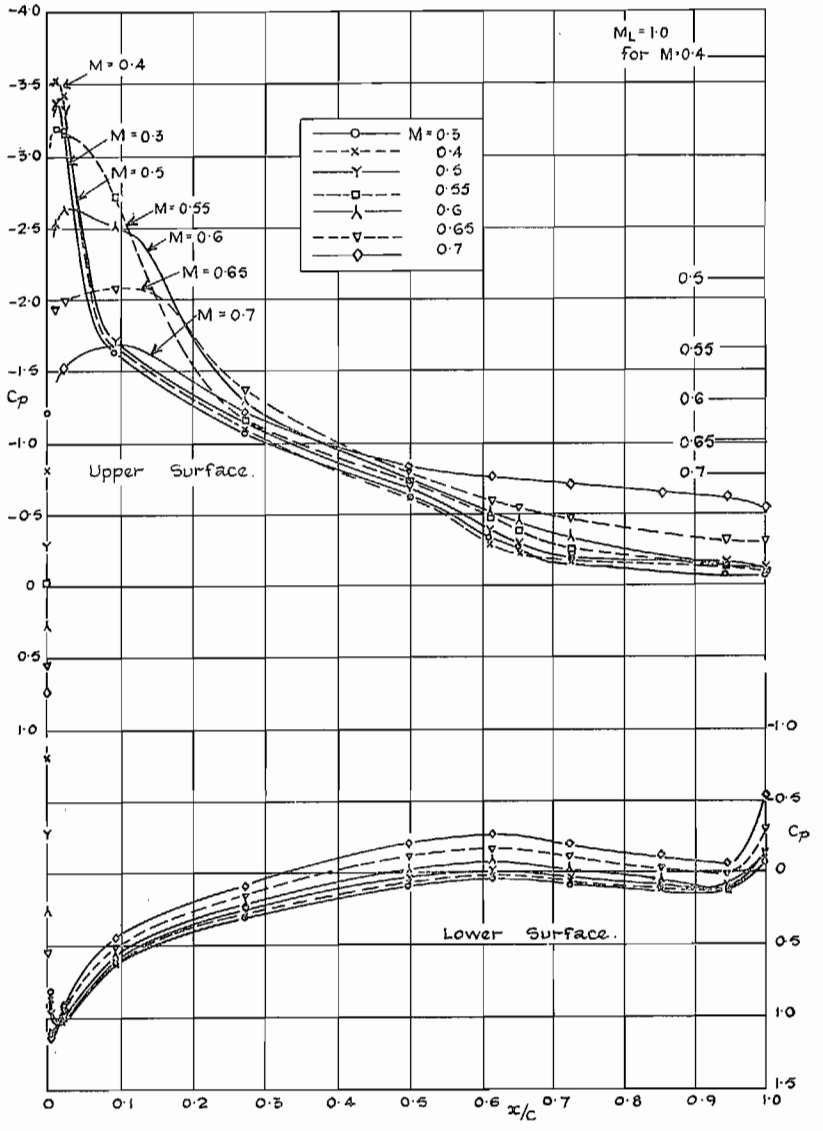

FIG. 8. Pressure distributions for various Mach numbers at 10·5 deg incidence.

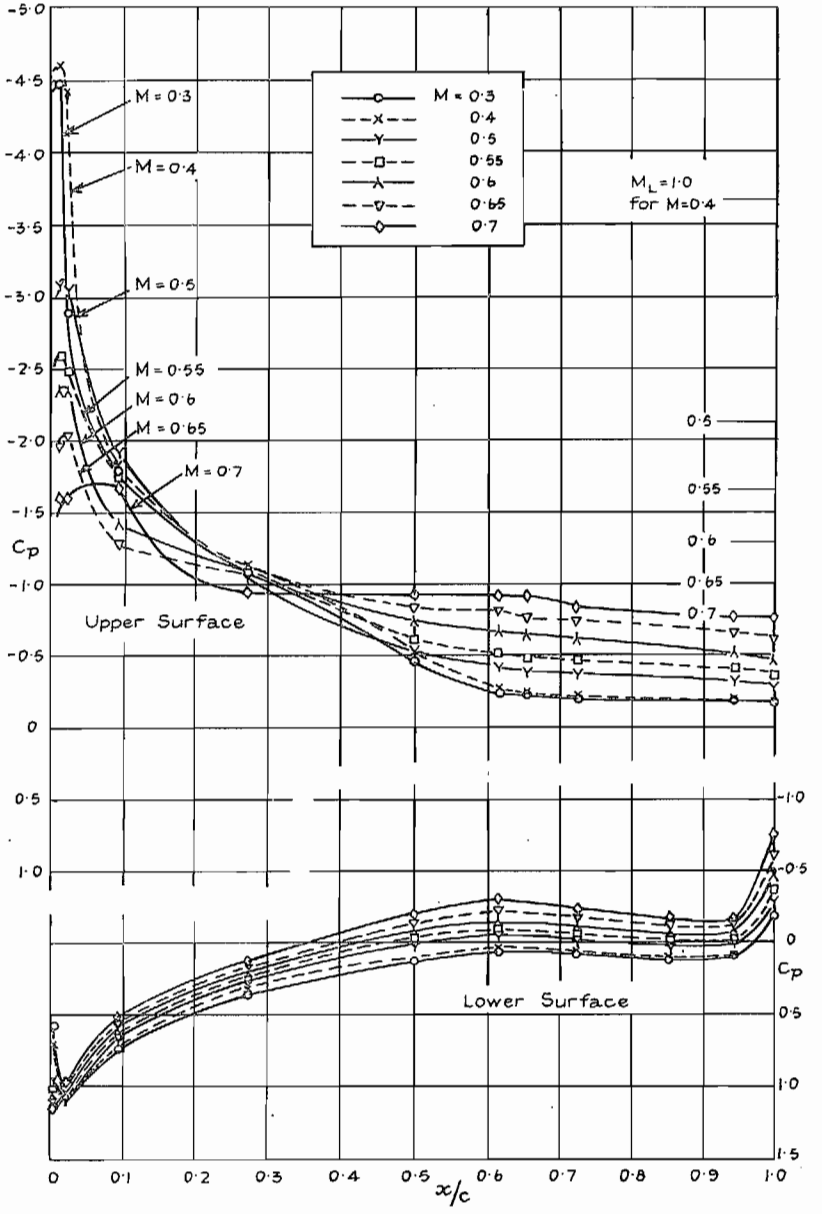

FIG. 9. Pressure distributions for various Mach numbers at 12·5 deg incidence.

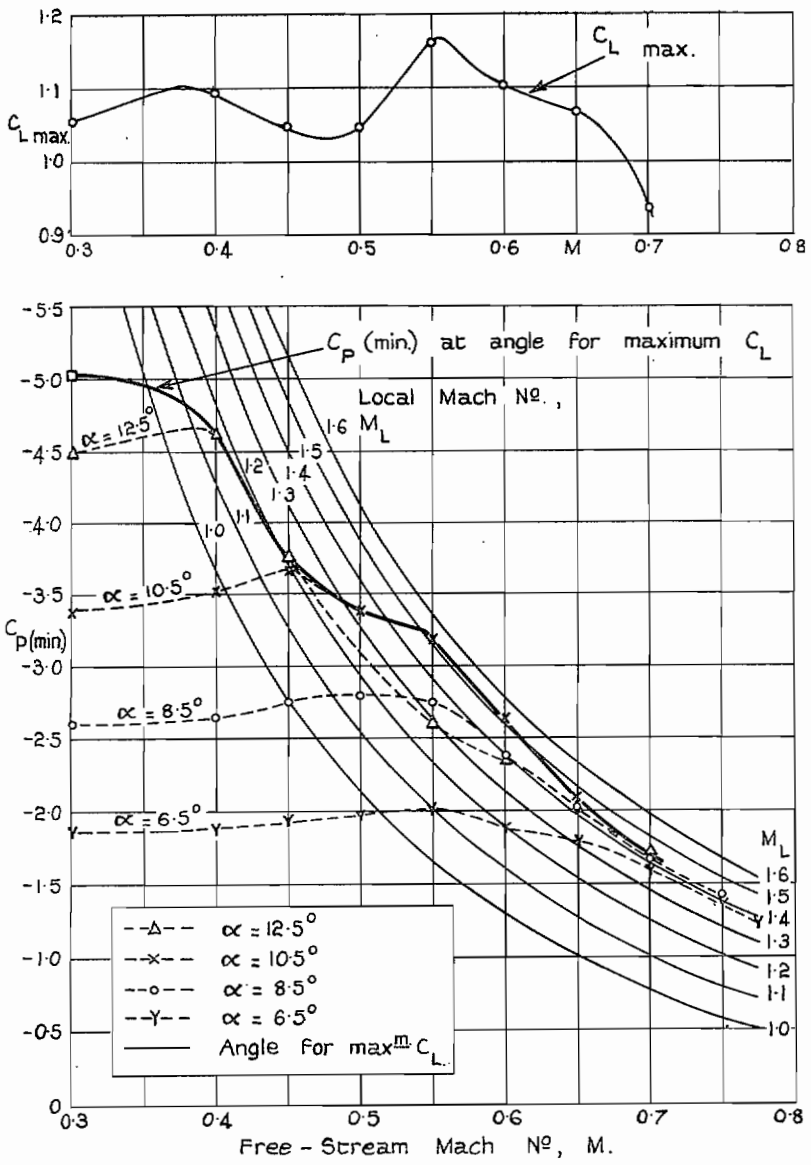

FIG. 10. Variation with Mach number of the minimum pressure coefficient on the upper surface for high incidences.

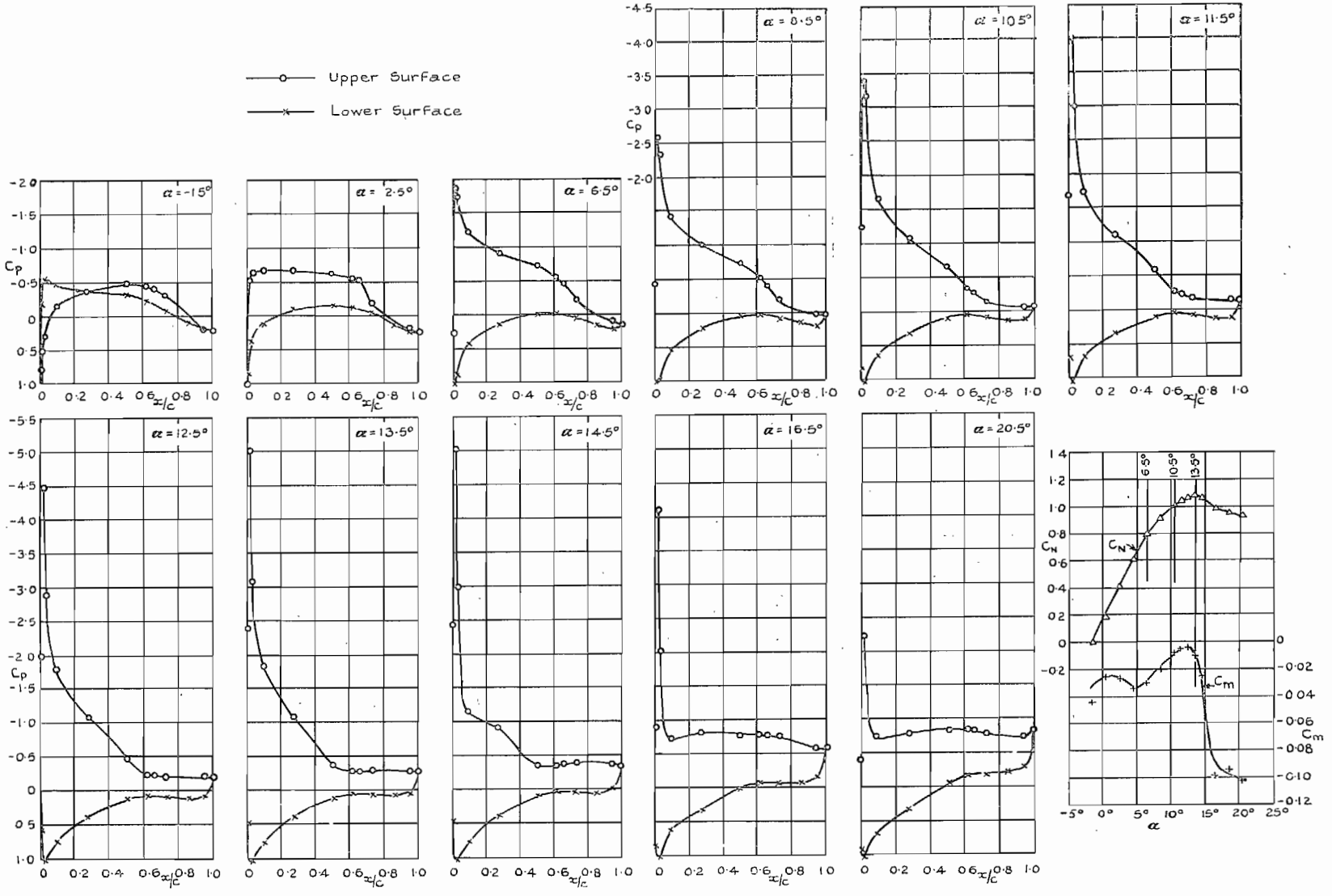

FIG. 11. Pressure distributions for $M = 0{\cdot}3$.

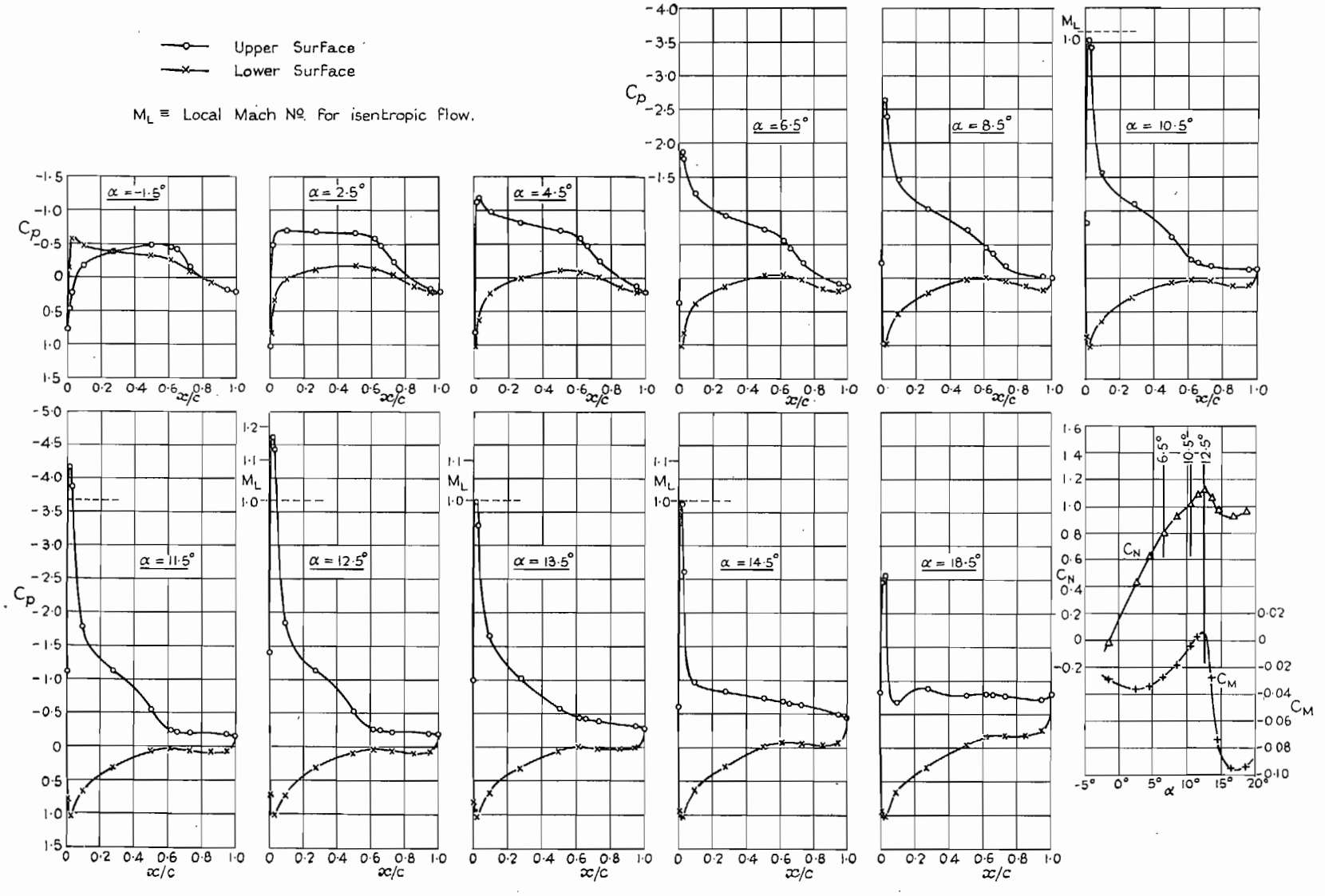

FIG. 12a. Pressure distributions for $M = 0{\cdot}4$.

$\alpha = 10{\cdot}5°$ $\alpha = 12{\cdot}5°$ $\alpha = 13{\cdot}5°$

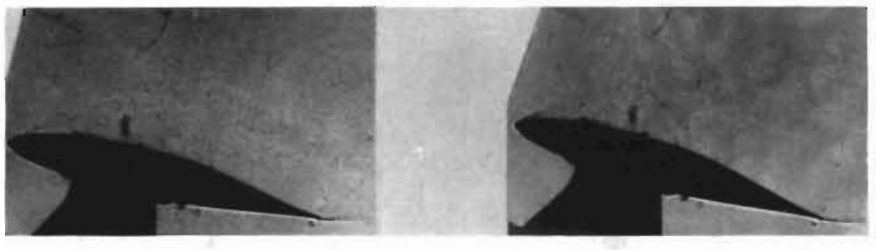

$\alpha = 14{\cdot}5°$ $\alpha = 18{\cdot}5°$

FIG. 12b. Direct-shadow photographs for $M = 0{\cdot}4$.

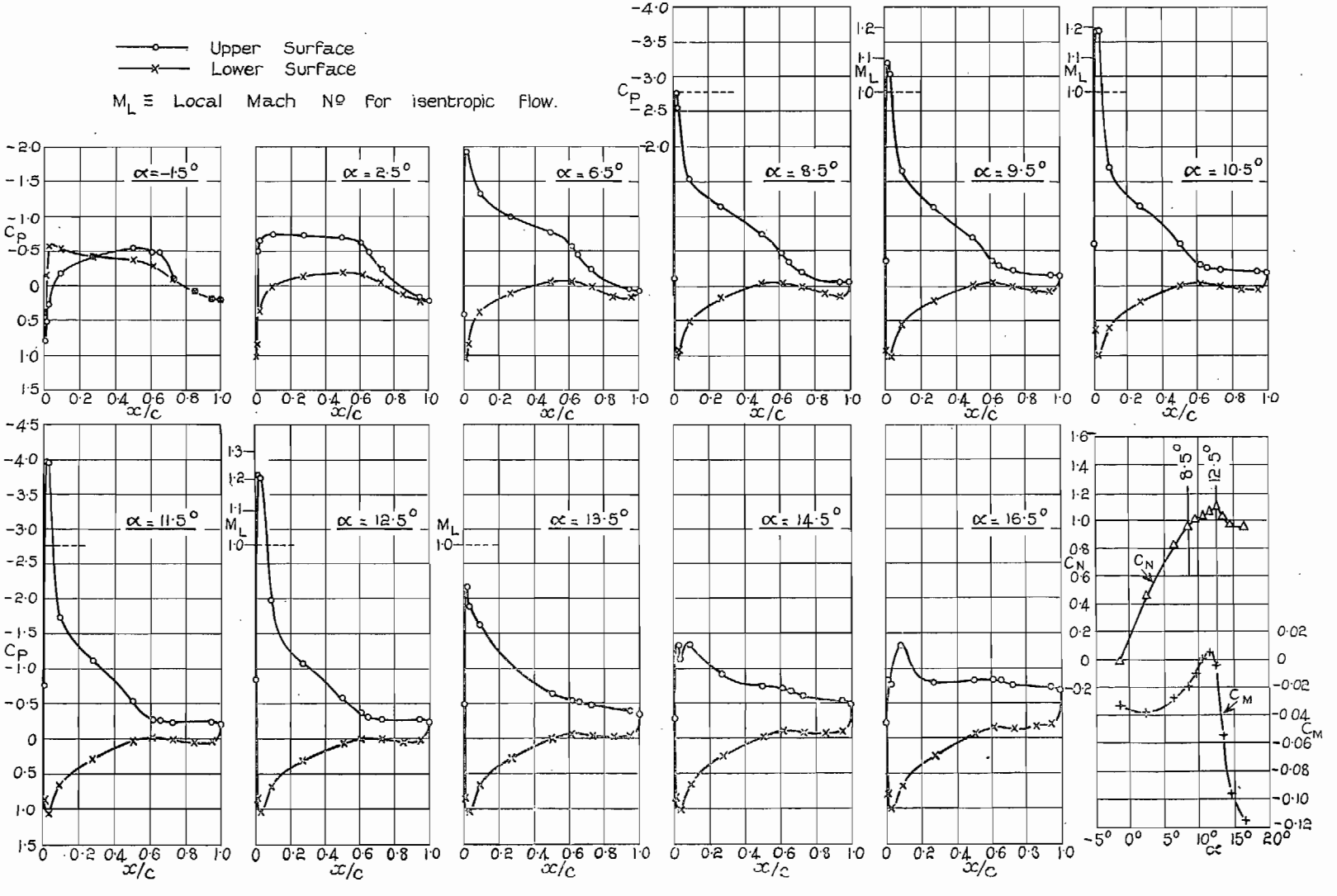

FIG. 13. Pressure distributions for $M = 0{\cdot}45$.

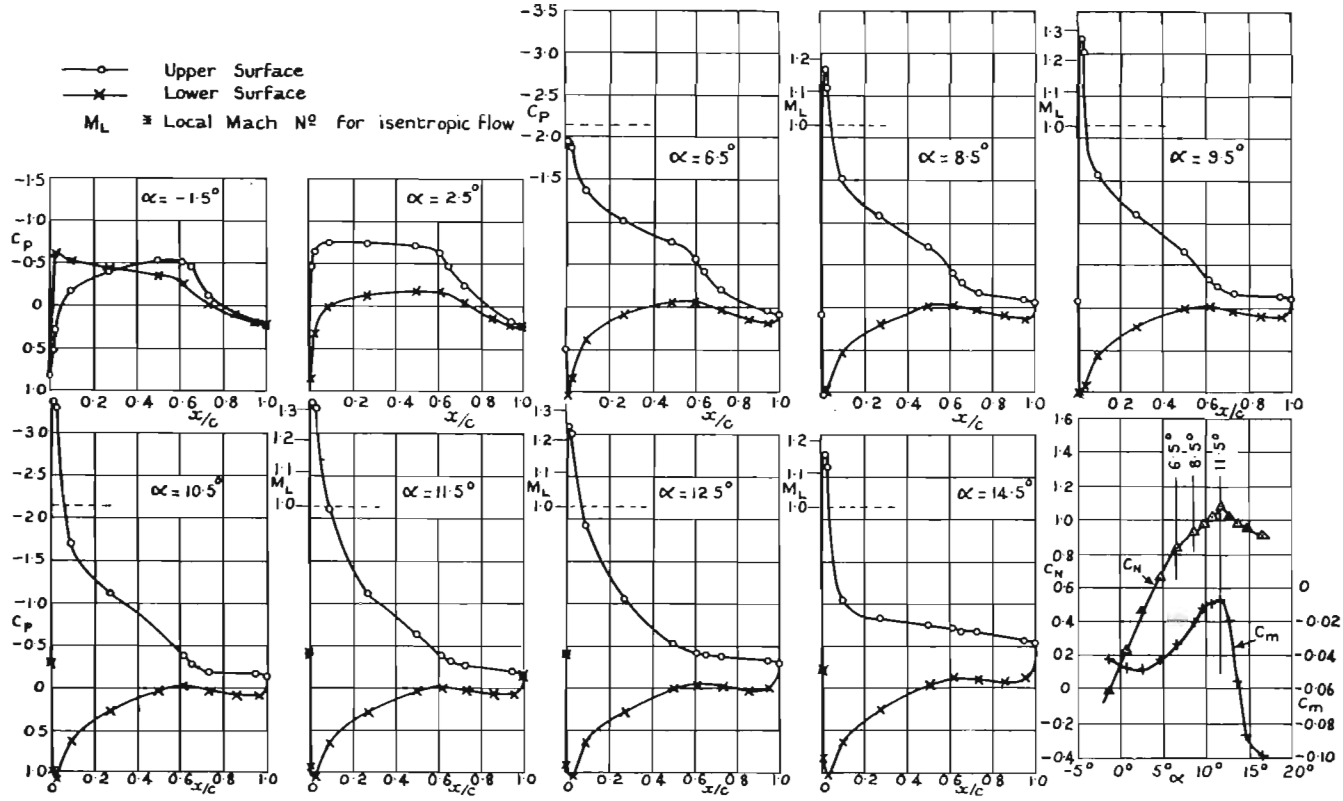

FIG. 14a. Pressure distributions for $M = 0{\cdot}5$.

$\alpha = 8{\cdot}5°$ $\alpha = 10{\cdot}5°$ $\alpha = 11{\cdot}5°$

$\alpha = 12{\cdot}5°$ $\alpha = 14{\cdot}5°$

FIG. 14b. Direct-shadow photographs for $M = 0{\cdot}5$.

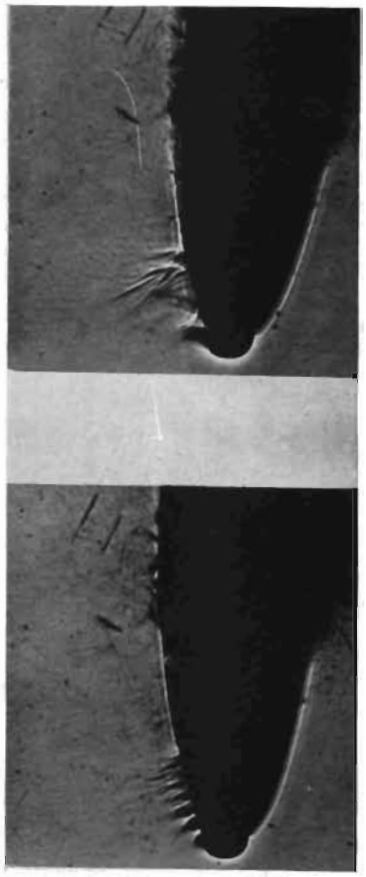

FIG. 14c. Direct-shadow photographs (enlarged) : $M = 0{\cdot}5$.

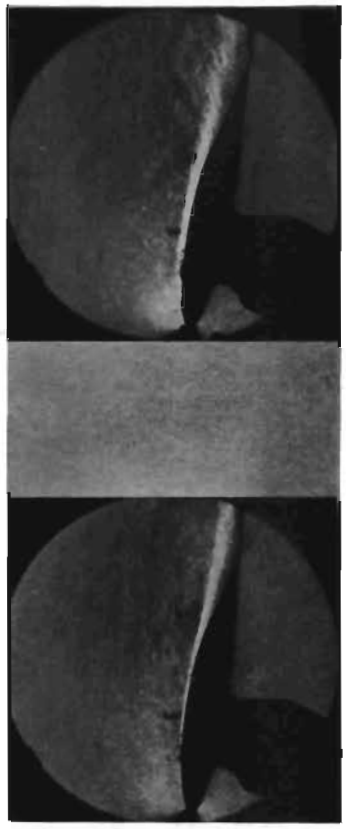

FIG. 14d. Schlieren photographs : $M = 0{\cdot}5$.

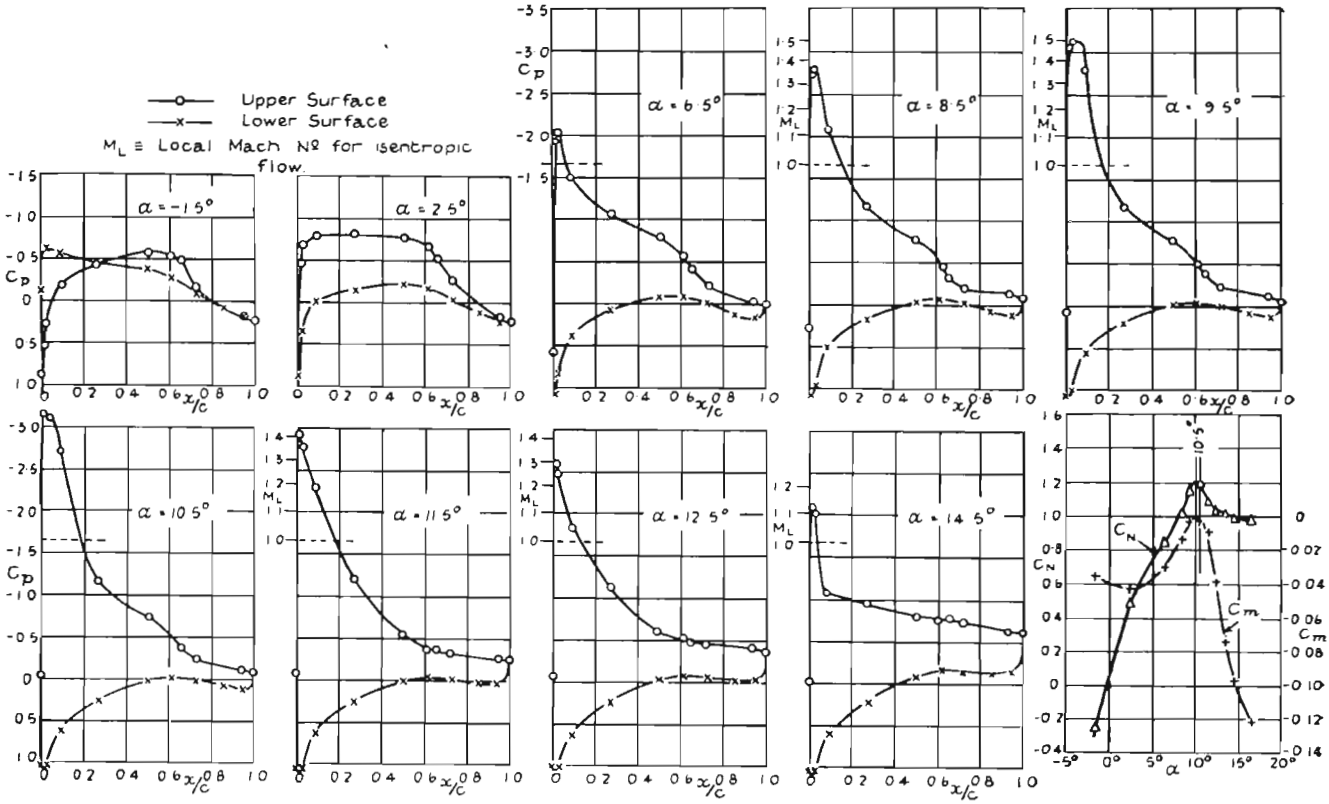

FIG. 15. Pressure distributions for $M = 0{\cdot}55$.

DI

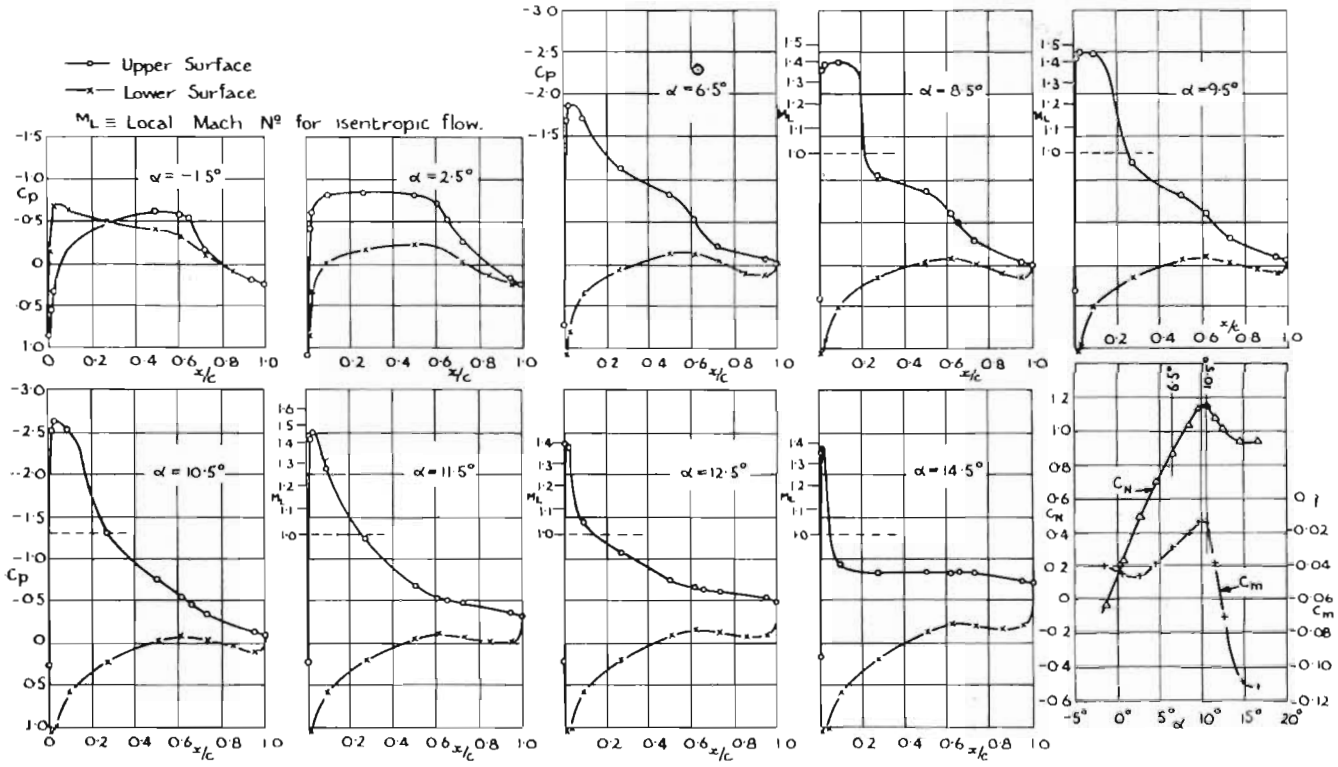

FIG. 16a. Pressure distribution for $M = 0{\cdot}6$.

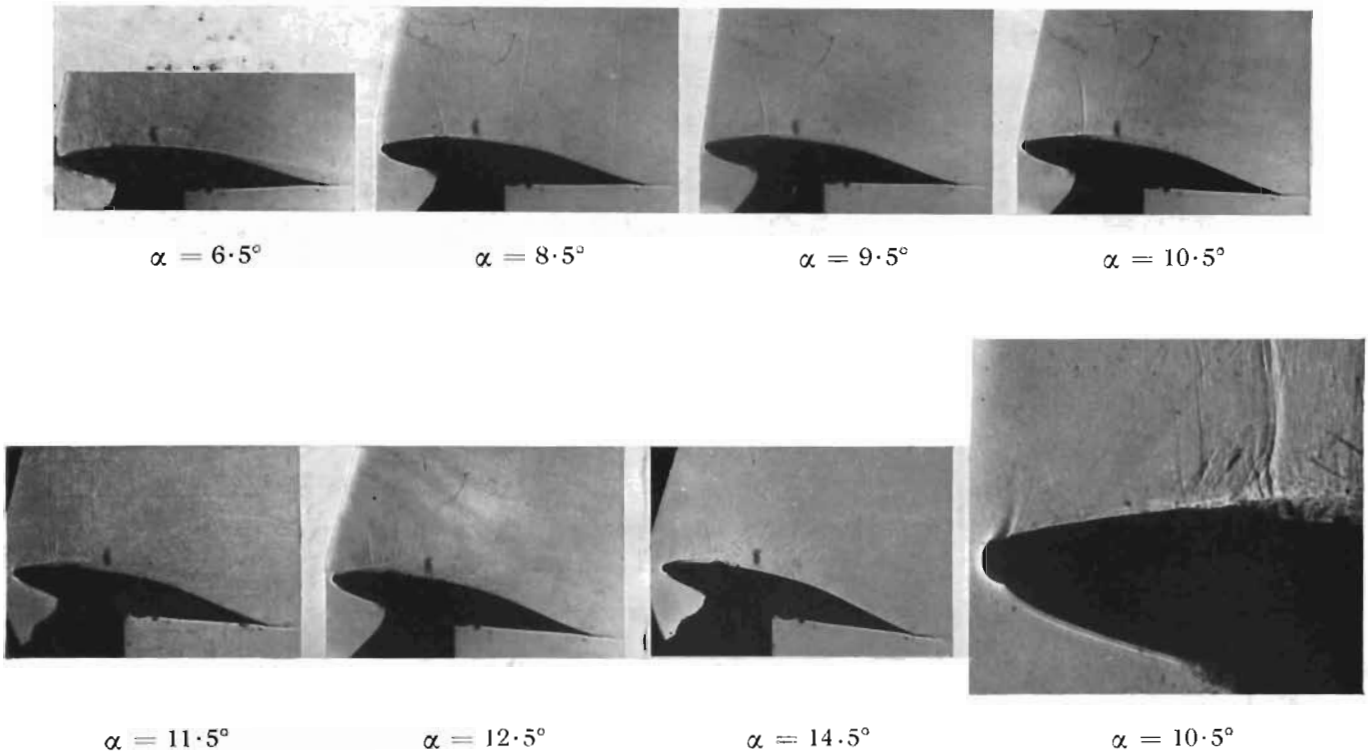

FIG. 16b. Direct-shadow photographs for $M = 0{\cdot}6$.

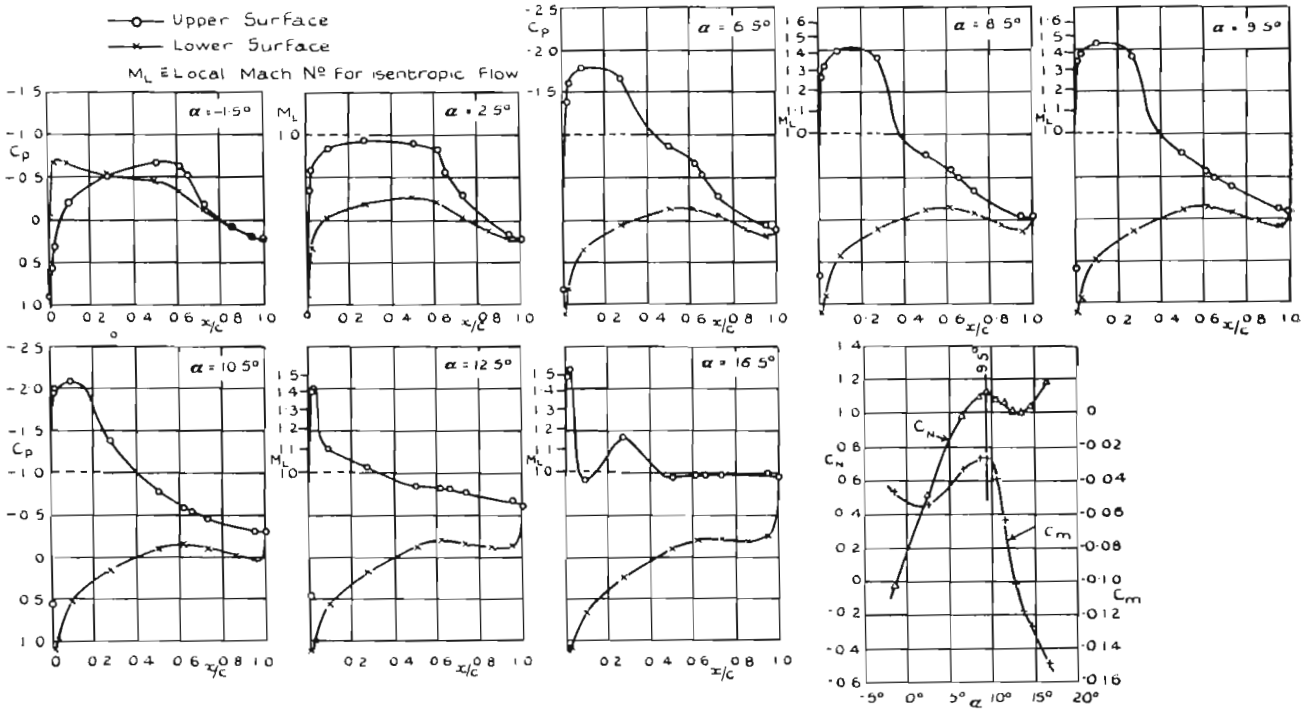

FIG. 17a. Pressure distributions for $M = 0{\cdot}65$.

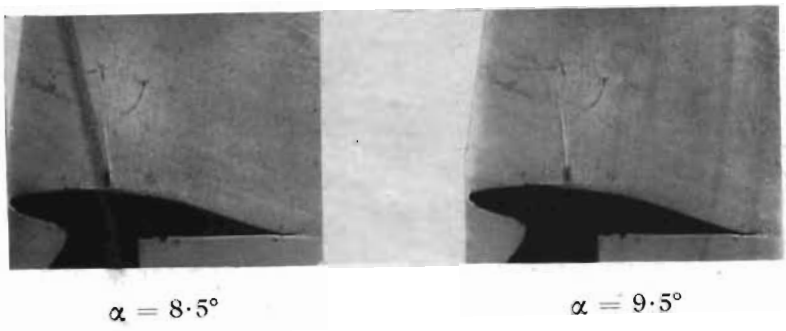

$\alpha = 8{\cdot}5°$ $\alpha = 9{\cdot}5°$

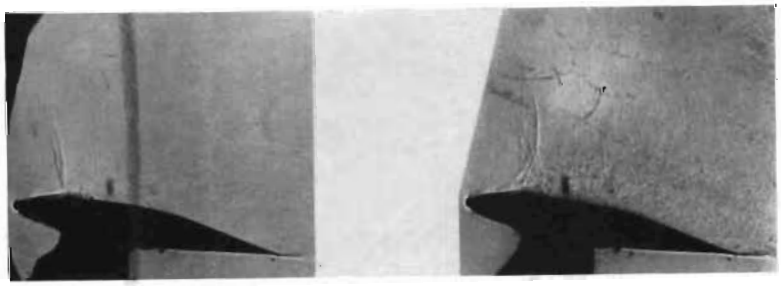

$\alpha = 10{\cdot}5°$ $\alpha = 12{\cdot}5°$

FIG. 17b. Direct-shadow photographs for $M = 0{\cdot}65$.

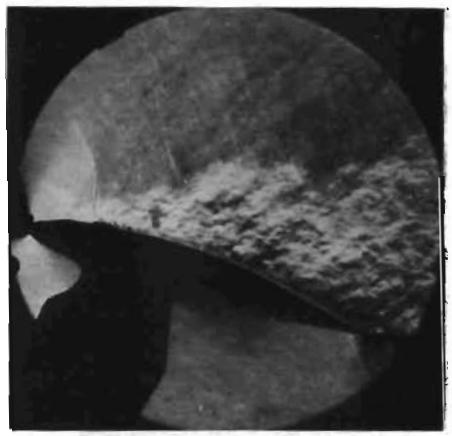

FIG. 17c. Schlieren photograph for $M = 0{\cdot}65$, $\alpha = 10{\cdot}5$ deg.

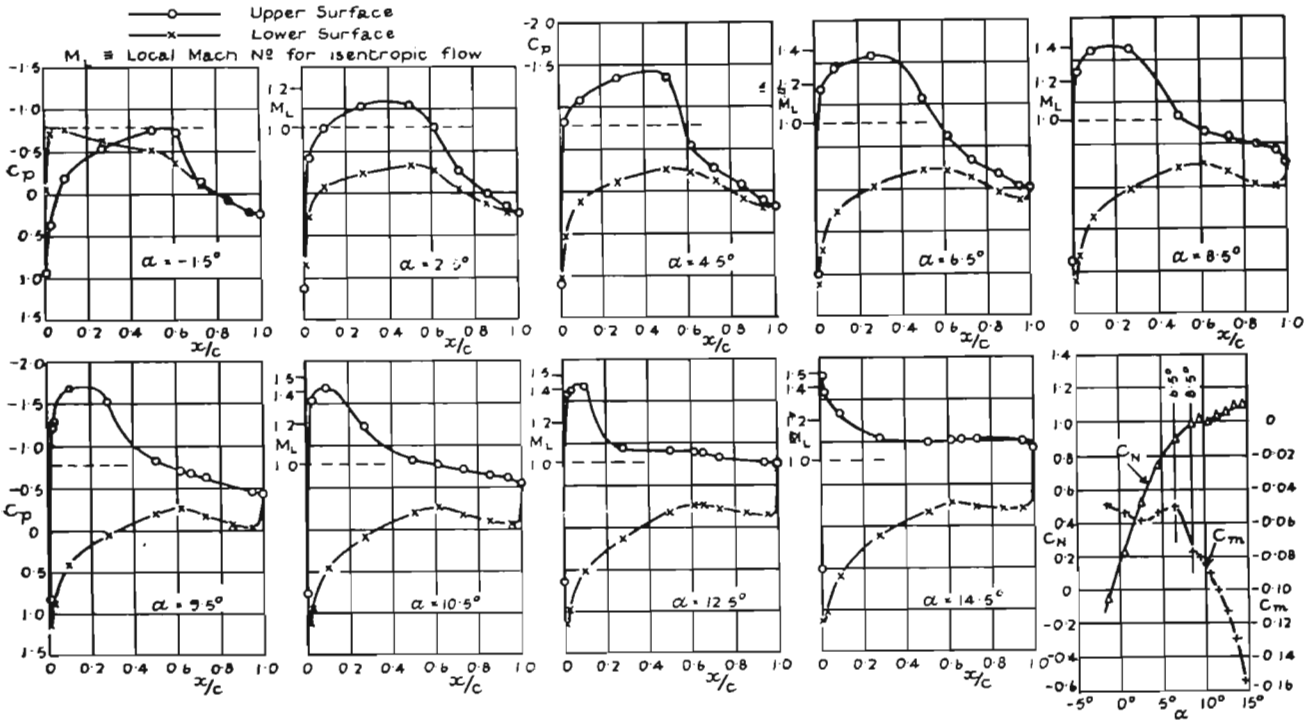

FIG. 18a. Pressure distributions for $M = 0{\cdot}7$.

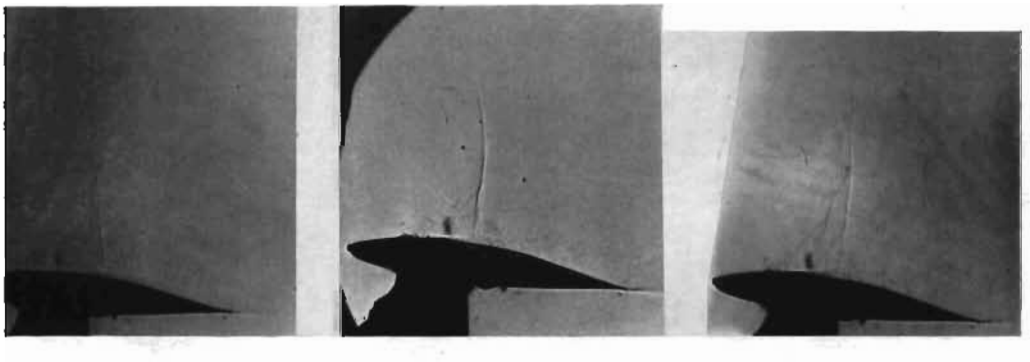

$\alpha = 6{\cdot}5°$ $\alpha = 8{\cdot}5°$ $\alpha = 9{\cdot}5°$

$\alpha = 10{\cdot}5°$ $\alpha = 12{\cdot}5°$ $\alpha = 14{\cdot}5°$

FIG. 18b. Direct-shadow photographs for $M = 0{\cdot}7$.

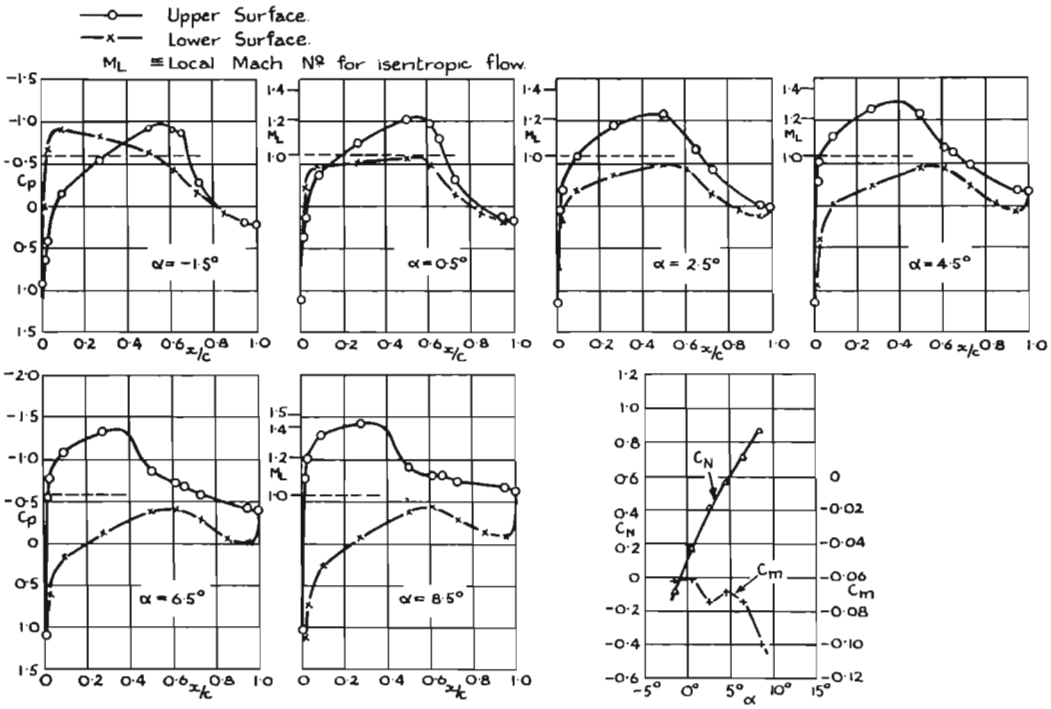

FIG. 19a. Pressure distributions for $M = 0{\cdot}75$. Incidences up to 8·5 deg.

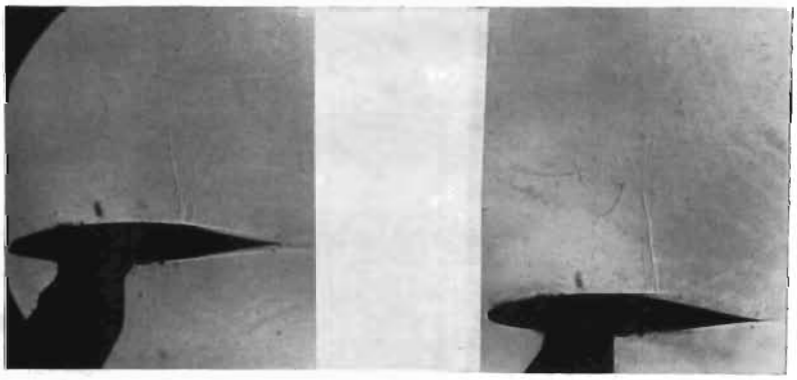

$\alpha = -1{\cdot}5°$ $\qquad$ $\alpha = 2{\cdot}5°$

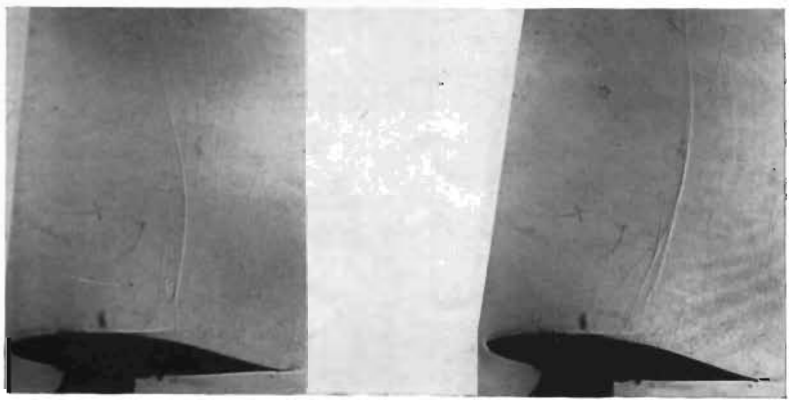

$\alpha = 6{\cdot}5°$ $\qquad$ $\alpha = 8{\cdot}5°$

FIG. 19b. Direct-shadow photographs for $M = 0{\cdot}75$. Incidences up to 8·5 deg.

(a)

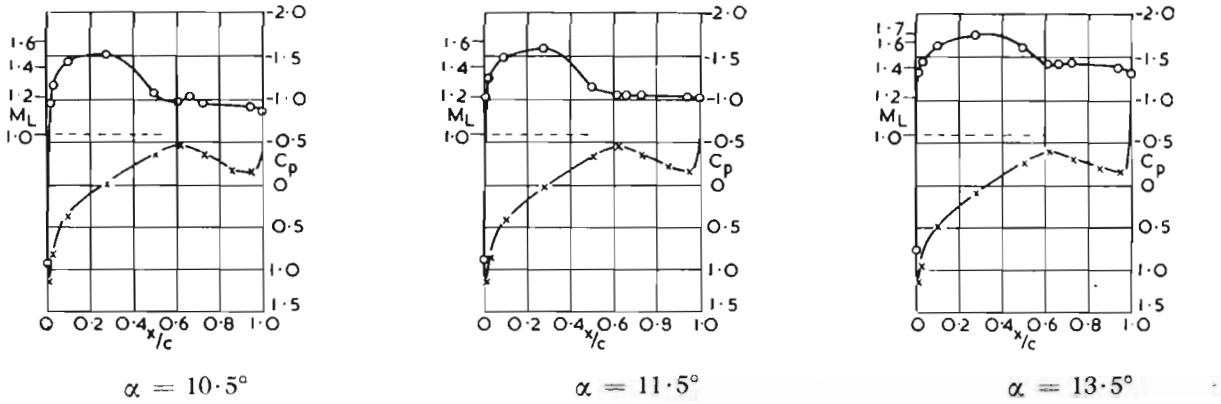

(b)

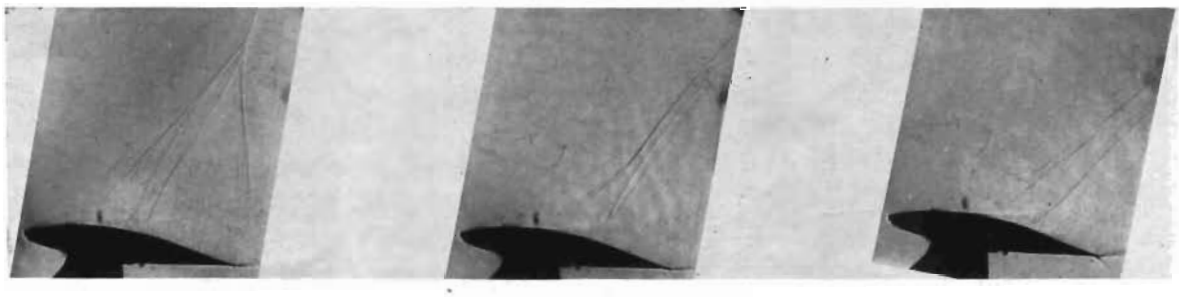

FIG. 20. Pressure distributions and photographs for $M = 0{\cdot}75$. Incidences above 8·5 deg (*see* section 3.2).

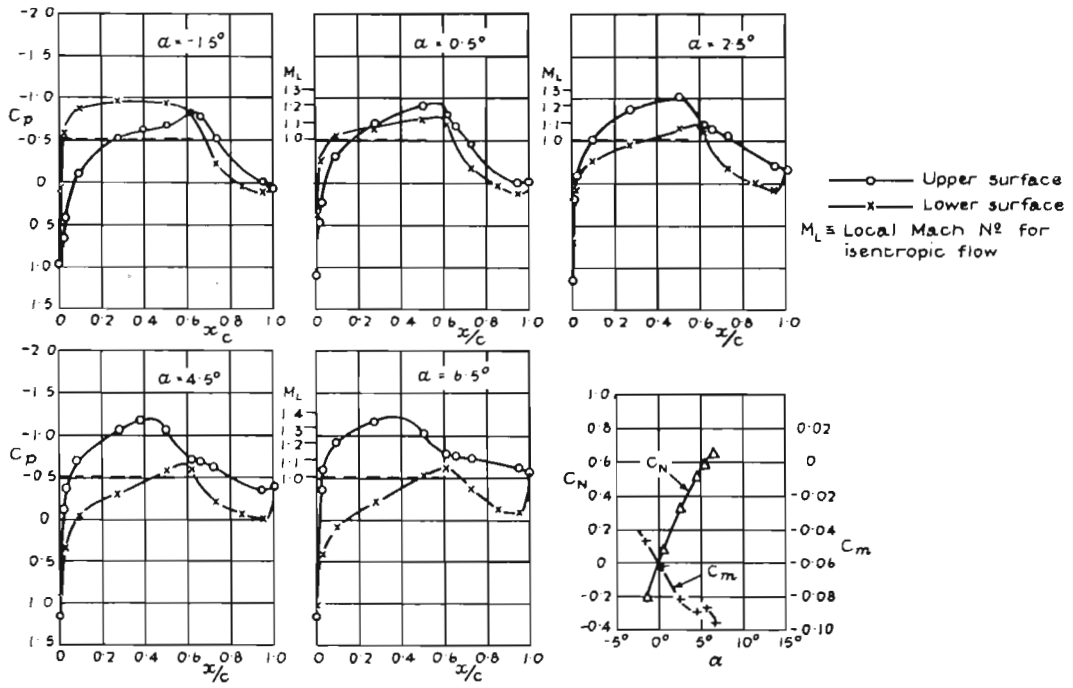

FIG. 21. Pressure distributions for $M = 0{\cdot}775$. Incidences up to 6·5 deg.

(a)

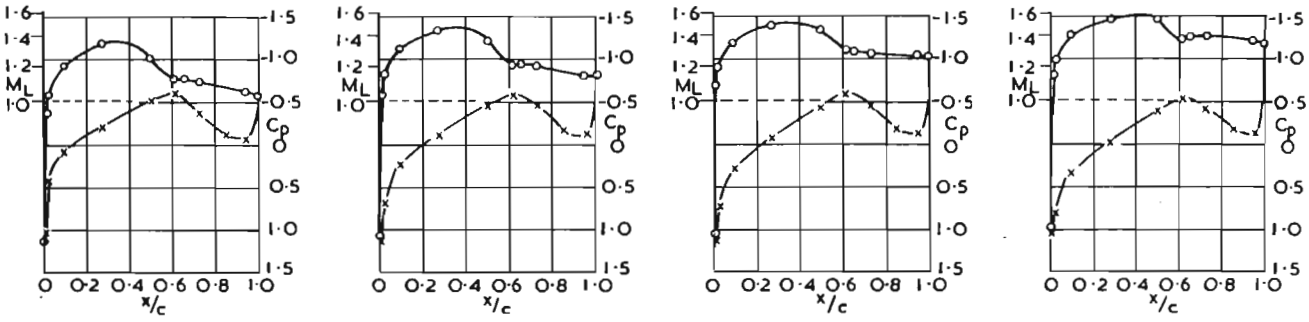

$\alpha = 6{\cdot}5°$ $\alpha = 8{\cdot}5°$ $\alpha = 9{\cdot}5°$ $\alpha = 10{\cdot}5°$

(b)

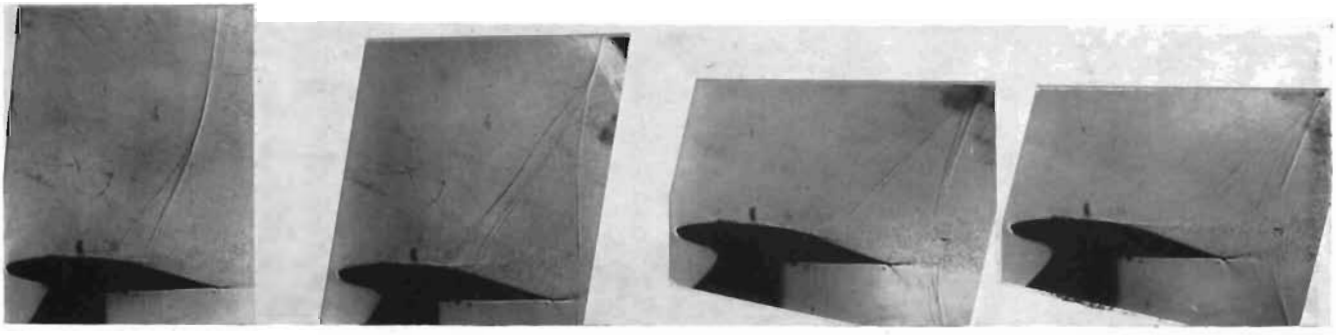

FIG. 22. Pressure distributions and photographs for $M = 0{\cdot}775$. Incidences of 6·5 deg and above (*see* section 3.2)

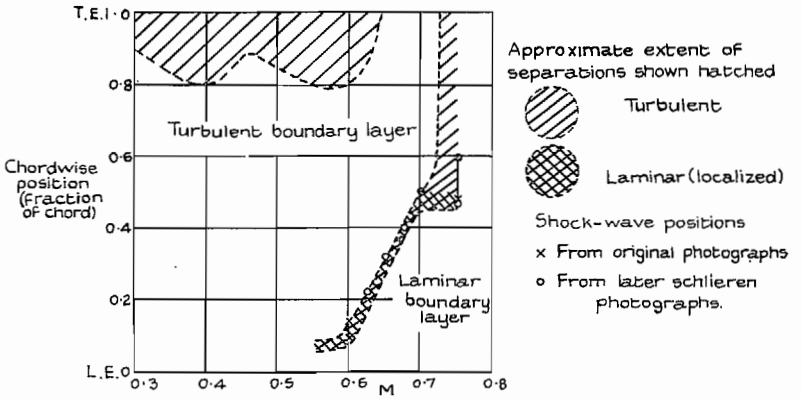

(a) Positions of boundary-layer separations and of shock-wave.

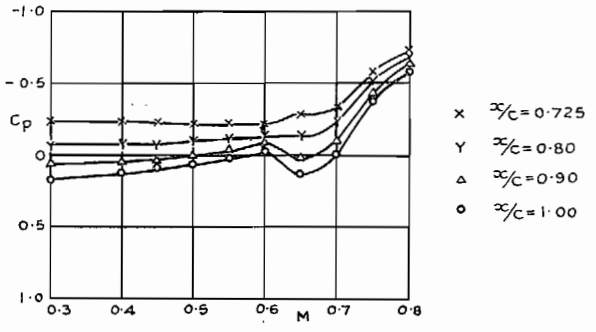

(b) Variation of surface pressures near the trailing edge.

FIG. 23. Observations of the flow over the upper surface. 6·5 deg incidence. Varying Mach number.

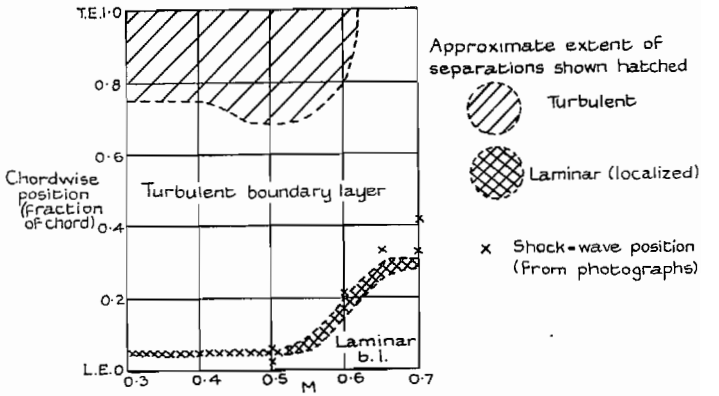

(a) Positions of boundary-layer separations and of shock-wave

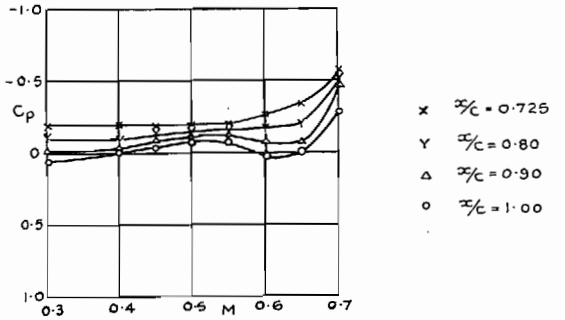

(b) Variation of surface pressures near the trailing edge.

FIG. 24. Observations of the flow over the upper surface. 8·5 deg incidence. Varying Mach number.

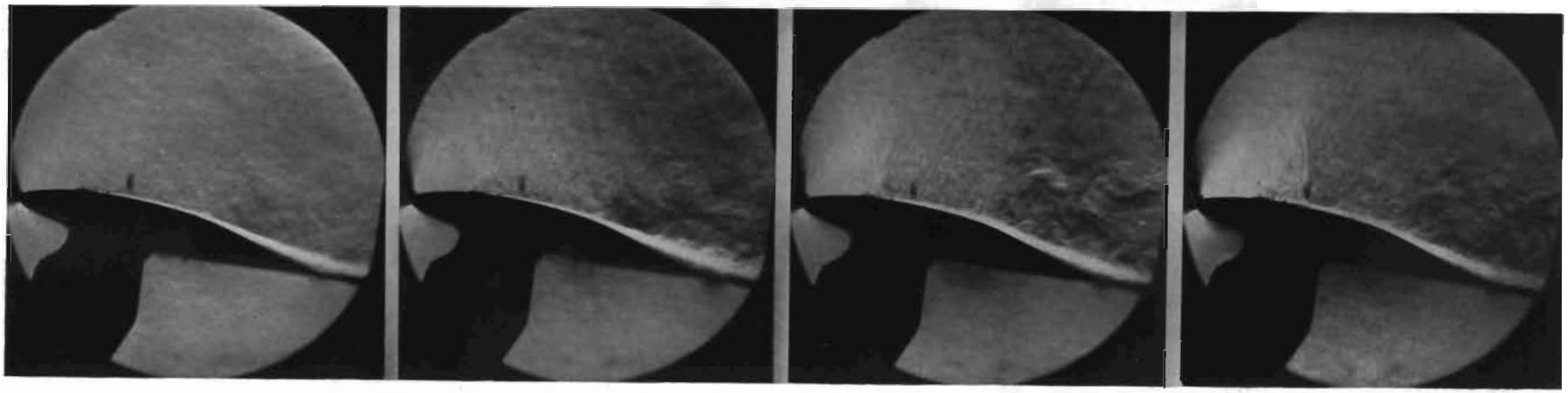

$M = 0{\cdot}5$ $M = 0{\cdot}6$ $M = 0{\cdot}625$ $M = 0{\cdot}65$

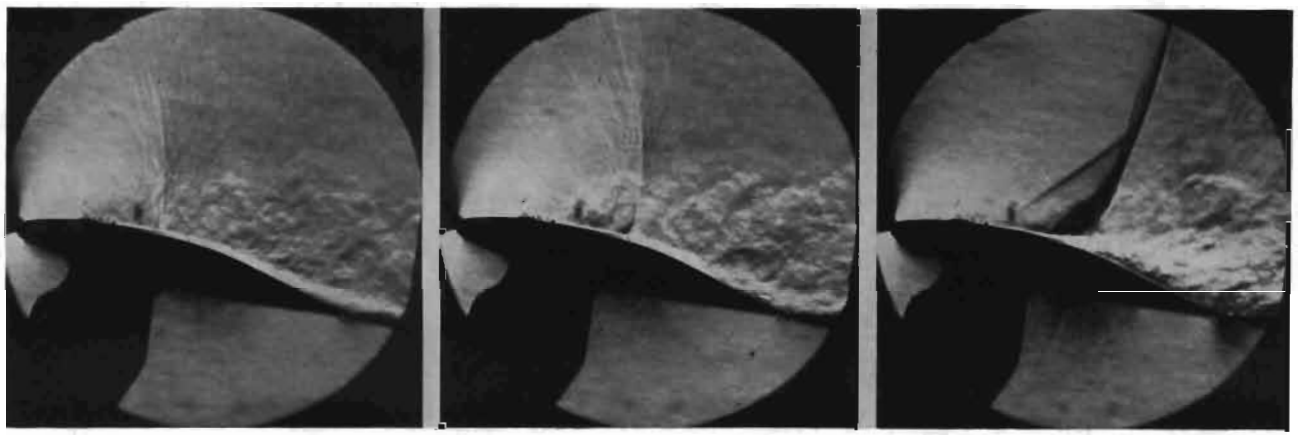

$M = 0{\cdot}675$ $M = 0{\cdot}70$ $M = 0{\cdot}75$

FIG. 25. Schlieren photographs for $\alpha = 6{\cdot}5$. Increasing Mach number.

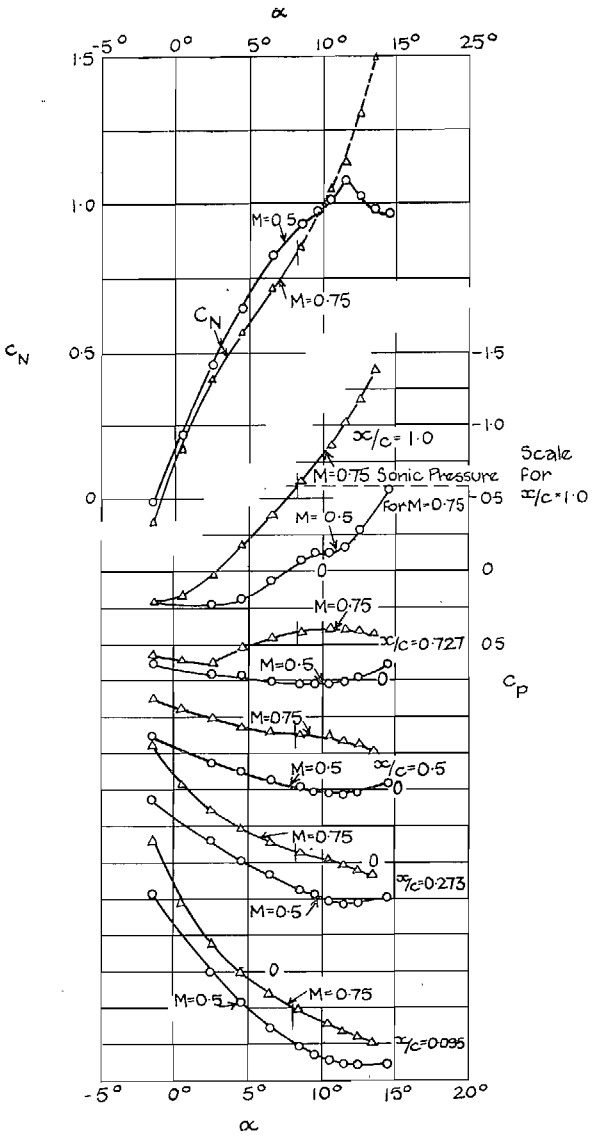

FIG. 26. Variation, with incidence, of pressure at fixed chordwise positions on the lower surface for $M = 0{\cdot}5$ and $0{\cdot}75$.

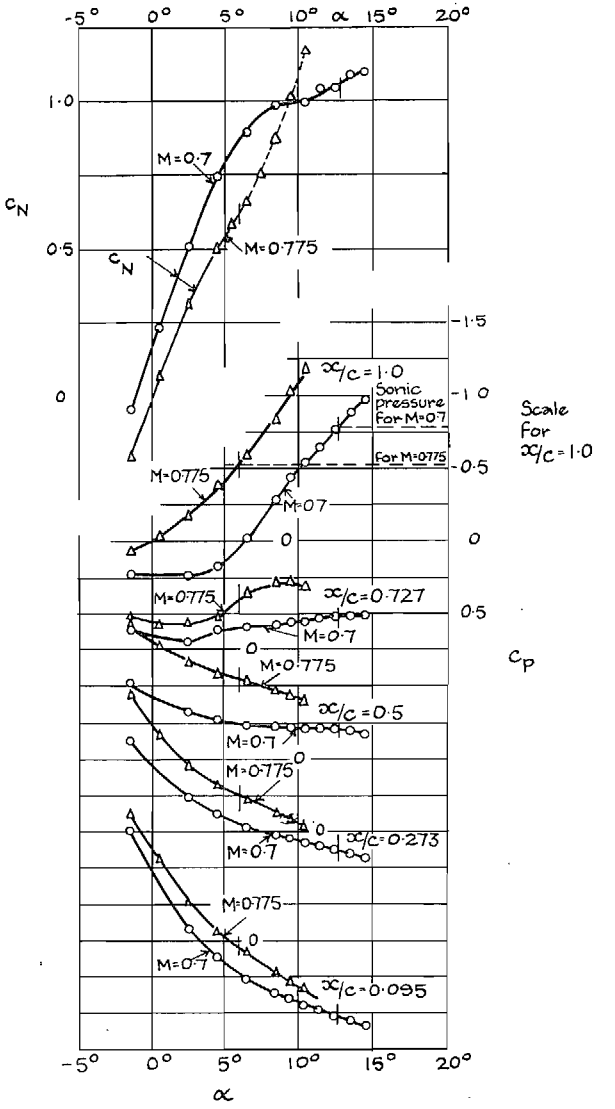

FIG. 27. Variation, with incidence, of pressures at fixed chordwise positions on the lower surface for $M = 0{\cdot}7$ and $0{\cdot}775$.

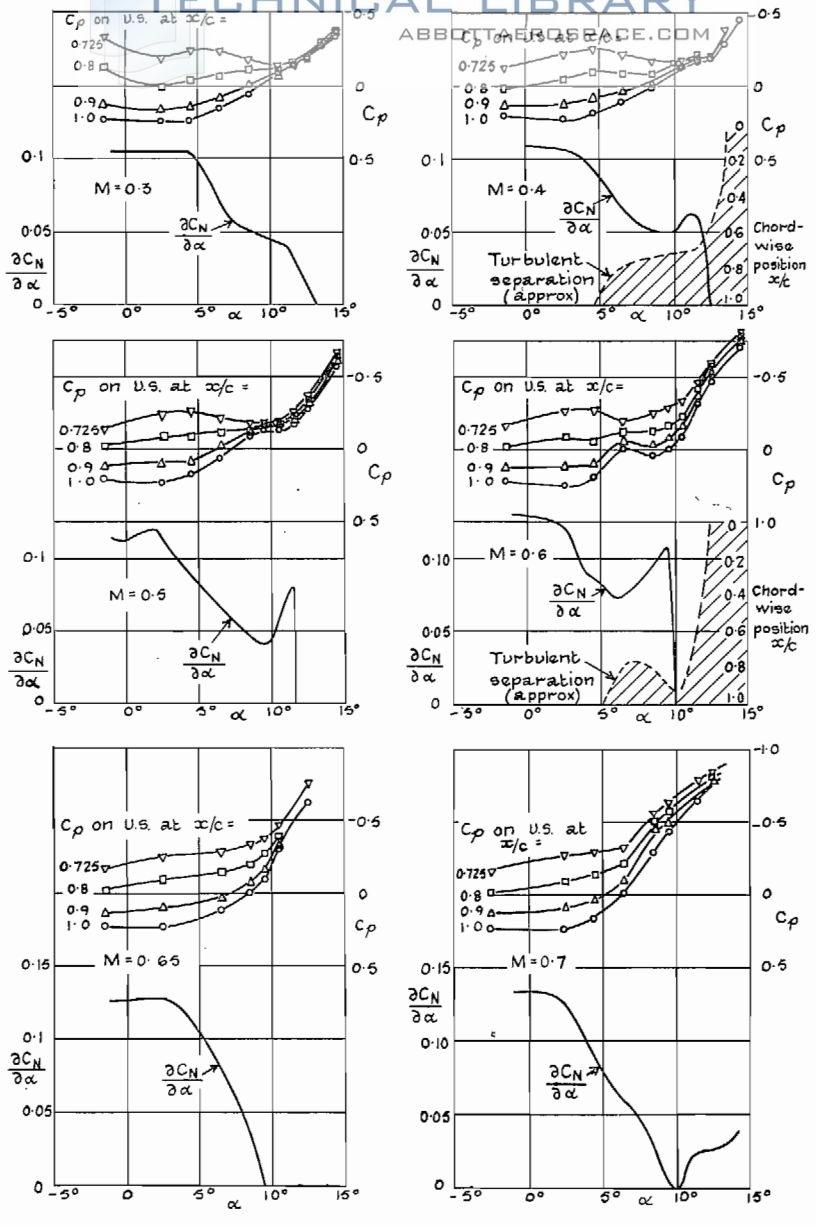

FIG. 28. Correlation between variations in lift-curve slope and pressures over the rear of the upper surface. Mach numbers up to 0·7.

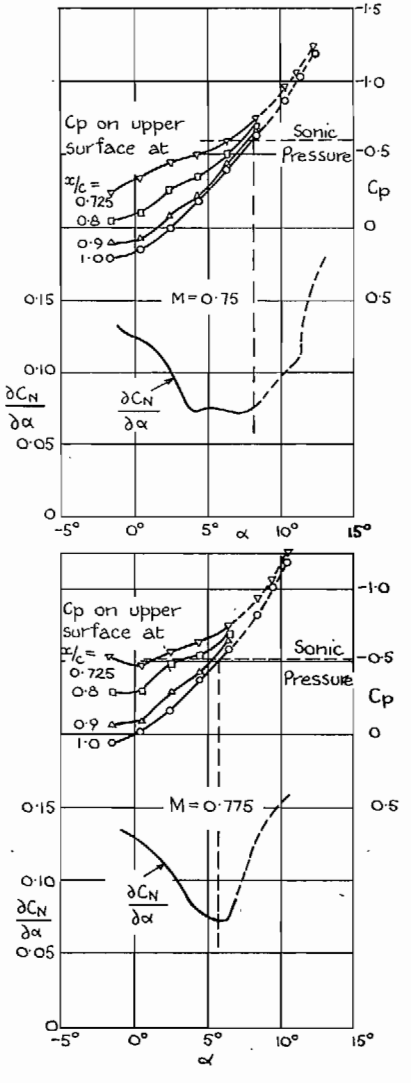

FIG. 29. Correlation between variations in lift-curve slope and pressures over the rear of the upper surface. $M = 0{\cdot}75$ and $0{\cdot}775$.

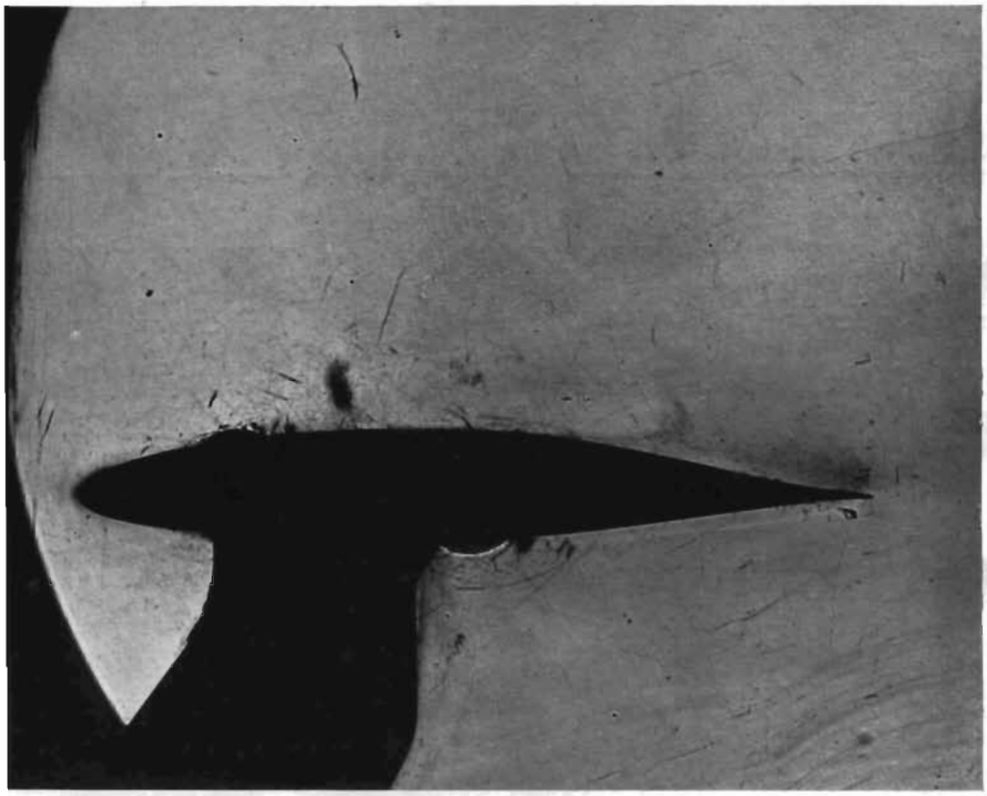

FIG. 30. Control direct-shadow photographs.

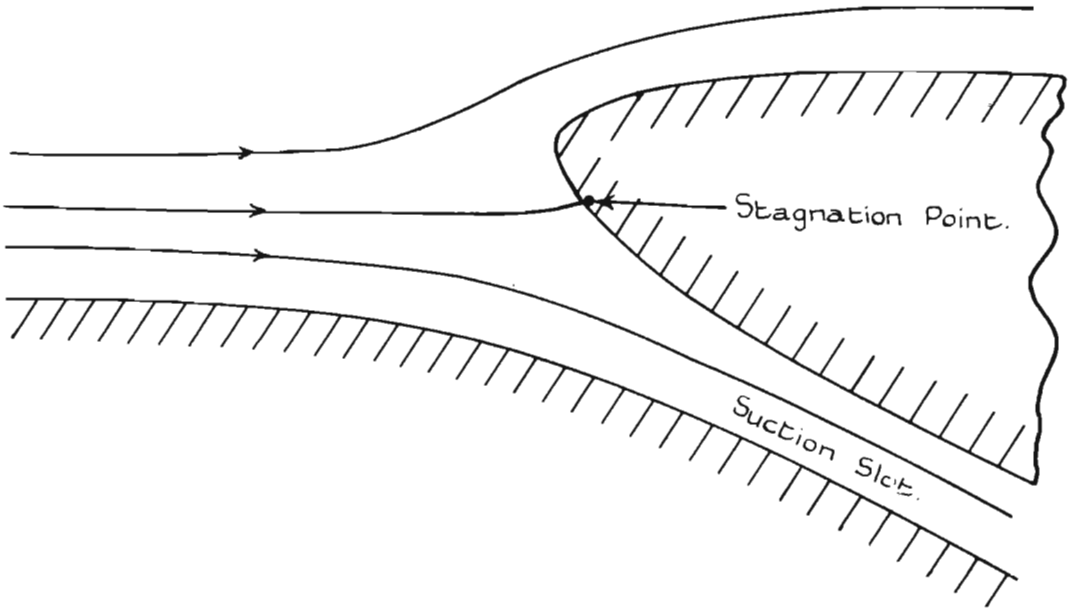

FIG. 31. Simulation of flow around the leading edge of an aerofoil.

J4308 Wt.17/1580 K9 1/55 D&Co. 34/263 PRINTED IN GREAT BRITAIN

Publications of the Aeronautical Research Council

ANNUAL TECHNICAL REPORTS OF THE AERONAUTICAL RESEARCH COUNCIL (BOUND VOLUMES)

1936 Vol. I. Aerodynamics General, Performance, Airscrews, Flutter and Spinning. 40*s.* (41*s.* 1*d*).

Vol. II. Stability and Control, Structures, Seaplanes, Engines, etc. 50*s.* (51*s.* 1*d.*)

1937 Vol. I. Aerodynamics General, Performance, Airscrews, Flutter and Spinning. 40*s.* (41*s.* 1*d.*)

Vol. II. Stability and Control, Structures, Seaplanes, Engines, etc. 60*s.* (61*s.* 1*d.*)

1938 Vol. I. Aerodynamics General, Performance, Airscrews. 50*s.* (51*s.* 1*d.*)

Vol. II. Stability and Control, Flutter, Structures, Seaplanes, Wind Tunnels, Materials. 30*s.* (31*s.* 1*d.*)

1939 Vol. I. Aerodynamics General, Performance, Airscrews, Engines. 50*s.* (51*s.* 1*d.*)

Vol. II. Stability and Control, Flutter and Vibration, Instruments, Structures, Seaplanes, etc. 63*s.* (64*s.* 2*d.*)

1940 Aero and Hydrodynamics, Aerofoils, Airscrews, Engines, Flutter, Icing, Stability and Control, Structures, and a miscellaneous section. 50*s.* (51*s.* 1*d.*)

1941 Aero and Hydrodynamics, Aerofoils, Airscrews, Engines, Flutter, Stability and Control, Structures. 63*s.* (64*s.* 2*d.*)

1942 Vol. I. Aero and Hydrodynamics, Aerofoils, Airscrews, Engines. 75*s.* (76*s.* 3*d.*)

Vol. II. Noise, Parachutes, Stability and Control, Structures, Vibration, Wind Tunnels. 47*s.* 6*d.* (48*s.* 7*d.*)

1943 Vol. I. Aerodynamics, Aerofoils, Airscrews, 80*s.* (81*s.* 4*d.*)

Vol. II. Engines, Flutter, Materials, Parachutes, Performance, Stability and Control, Structures. 90*s.* (91*s.* 6*d.*)

1944 Vol. I. Aero and Hydrodynamics, Aerofoils, Aircraft, Airscrews, Controls. 84*s.* (85*s.* 8*d.*)

Vol. II. Flutter and Vibration, Materials, Miscellaneous, Navigation, Parachutes, Performance, Plates, and Panels, Stability, Structures, Test Equipment, Wind Tunnels. 84*s.* (85*s.* 8*d.*)

ANNUAL REPORTS OF THE AERONAUTICAL RESEARCH COUNCIL—

1933–34	1*s.* 6*d.* (1*s.* 8*d.*)	1937	2*s.* (2*s.* 2*d.*)
1934–35	1*s.* 6*d.* (1*s.* 8*d.*)	1938	1*s.* 6*d.* (1*s.* 8*d.*)
April 1, 1935 to Dec. 31, 1936.	4*s.* (4*s.* 4*d.*)	1939–48	3*s.* (3*s.* 2*d.*)

INDEX TO ALL REPORTS AND MEMORANDA PUBLISHED IN THE ANNUAL TECHNICAL REPORTS, AND SEPARATELY—

April, 1950 – – – –	R. & M. No. 2600.	2*s.* 6*d.* (2*s.* 7½*d.*)

AUTHOR INDEX TO ALL REPORTS AND MEMORANDA OF THE AERONAUTICAL RESEARCH COUNCIL—

1909–1949 – – – – –	R. & M. No. 2570.	15*s.* (15*s.* 3*d.*)

INDEXES TO THE TECHNICAL REPORTS OF THE AERONAUTICAL RESEARCH COUNCIL—

December 1, 1936 — June 30, 1939.	R. & M. No. 1850.	1*s.* 3*d.* (1*s.* 4½*d.*)
July 1, 1939 — June 30, 1945.	R. & M. No. 1950.	1*s.* (1*s.* 1½*d.*)
July 1, 1945 — June 30, 1946.	R. & M. No. 2050.	1*s.* (1*s.* 1½*d.*)
July 1, 1946 — December 31, 1946.	R. & M. No. 2150.	1*s.* 3*d.* (1*s.* 4½*d.*)
January 1, 1947 — June 30, 1947.	R. & M. No. 2250.	1*s.* 3*d.* (1*s.* 4½*d.*)
July, 1951 – – – –	R. & M. No. 2350.	1*s.* 9*d.* (1*s.* 10½*d.*)

Prices in brackets include postage.

Obtainable from

HER MAJESTY'S STATIONERY OFFICE

York House, Kingsway, London W.C.2 ; 423 Oxford Street, London W.1 (Post Orders : P.O. Box No. 569, London S.E.1) ; 13A Castle Street, Edinburgh 2 ; 39 King Street, Manchester 2 ; 2 Edmund Street, Birmingham 3 ; 109 St. Mary Street, Cardiff ; Tower Lane, Bristol 1 ; 80 Chichester Street, Belfast OR THROUGH ANY BOOKSELLER

S.O. Code No. 23-2849